Subchronic alteration of vestibular hair cells in mice: implications for multisensory gaze stabilization

Louise Schenberg[1], *Aïda Palou*[2,3,4], François Simon[1,5], *Tess Bonnard*[1], *Charles-Elliot Barton*[1], *Desdemona Fricker*[1], *Michele Tagliabue*[1], *Jordi Llorens*[2,3,4*], *Mathieu Beraneck*[1,*]

1- Université Paris Cité, CNRS UMR 8002, INCC - Integrative Neuroscience and Cognition Center, F-75006, Paris, France.

2- Departament de Ciències Fisiològiques, Universitat de Barcelona, 08907 l'Hospitalet de Llobrega, Catalunya, Spain.

3- Institut de Neurociènces, Universitat de Barcelona, Barcelona, Catalunya, Spain.

4- Institut d'Investigació Biomèdica de Bellvitge (IDIBELL), 08907 l'Hospitalet de Llobregat, Catalunya, Spain.

5- Department of paediatric otolaryngology, Hôpital Necker-Enfants Malades, APHP, F-75015, Paris, France.

*** Corresponding authors:**

Pr Jordi Llorens, Universitat de Barcelona, 08907 l'Hospitalet de Llobrega,, Catalunya, Spain. E-mail : jllorens@ub.edu

Dr. M. Beraneck. CNRS UMR 8002, Université Paris Cité, 45 rue des St-Pères, Paris 75270, France. Email: mathieu.beraneck@cnrs.fr

Funding: This work is supported by the Centre National d'Etudes Spatiales, the Centre National de la Recherche Scientifique, and the Université Paris Cité. MB and LS received funding from the Agence Nationale de la Recherche (ANR-20-CE37-0016 INVEST). MB, FS & DF received funding from the ERANET NEURON Program VELOSO (ANR-20-NEUR-0005). AP & JL received funding from the ERANET NEURON Program VELOSO (grant PCI2020-120681-2 from MCIN/ AEI/10.13039/501100011033 and NextGenerationEU/PRTR).

Acknowledgment: this study contributes to the IdEx Université de Paris ANR-18-IDEX-0001. This work has benefited from the support and expertise of the animal facility of BioMedTech Facilities at Université Paris Cité (Institut National de la Santé et de la Recherche Médicale Unité S36/Unité Mixte de Service 2009).

Author contribution: Conceptualization: JL ; MB. Methodology: LS ; AP ; FS ; MT ; JL ; MB. Formal analysis: LS ; AP ; MT ; JL ; MB. Investigation: LS ; AP ; TB ; CEB . Writing original

manuscript: LS ; MT ; MB. Writing review and editing: LS ; AP ; FS ; DF ; MT ; JL ; MB. Visualization: LS ; AP ; TB; MT ; JL ; MB. Supervision: LS ; DF ; MT ; JL ; MB. Project administration: JL; MB. Funding acquisition: DF, JL; MB.

Declaration of interests: The authors declare no competing interests.

Abstract

The functional complementarity of the vestibulo-ocular reflex (VOR) and optokinetic reflex (OKR) allows for optimal combined gaze stabilization responses (CGR) in light. While sensory substitution has been reported following complete vestibular loss, the capacity of the central vestibular system to compensate for partial peripheral vestibular loss remains to be determined. Here, we first demonstrate the efficacy of a 6-week subchronic ototoxic protocol in inducing transient and partial vestibular loss which equally affects the canal- and otolith-dependent VORs. Immunostaining of hair cells in the vestibular sensory epithelia revealed that organ-specific alteration of type I, but not type II, hair cells correlates with functional impairments. The decrease in VOR performance is paralleled with an increase in the gain of the OKR occurring in a specific range of frequencies where VOR normally dominates gaze stabilization, compatible with a sensory substitution process. Comparison of unimodal OKR or VOR versus bimodal CGR revealed that visuo-vestibular interactions remain reduced despite a significant recovery in the VOR. Modeling and sweep-based analysis revealed that the differential capacity to optimally combine OKR and VOR correlates with the reproducibility of the VOR responses. Overall, these results shed light on the multisensory reweighting occurring in pathologies with fluctuating peripheral vestibular malfunction.

Introduction

The vestibular system is well-preserved amongst vertebrates, participating in essential functions such as balance, postural control and, together with the optokinetic system, gaze stabilization (Straka et al., 2016; Wibble et al., 2022). Beyond these recognized roles, vestibular signals also contribute to cognitive processes e.g spatial orientation and navigation (Cullen, 2019), or body representation (Lopez et al., 2012; Facchini et al., 2021). Because of its involvement in many basic functions important in our daily life, vestibular pathologies affecting the inner ear are associated with a significant deterioration of the well-being of patients (Möhwald et al., 2020) and represent an important public health concern (Agrawal et al., 2009, 2013).

Research on post-lesion plasticity following permanent vestibular loss has shed light on the neural plastic mechanisms that follow a chronic unilateral or bilateral vestibular lesion, a process referred as "vestibular compensation" (Brandt et al., 1997; Cullen et al., 2010; Beraneck and Idoux, 2012). The compensation taking place after the lesion is known to involve dynamical multisensory reweighting of proprioceptive and visual inputs and of internal efferent copies (Cullen et al., 2010; Sadeghi et al., 2012; Sadeghi and Beraneck, 2020). While total and permanent lesions offer the experimental opportunity to characterize drastic cellular and molecular changes triggered by the total silencing of the vestibular endorgans, they imperfectly mimic clinical situations where peripheral vestibular function loss is only partial and/or transient (Bisdorff et al., 2009; Lopez-Escamez et al., 2015; Brandt and Dieterich, 2017). To better model fluctuating inner ear function, protocols based on subchronic exposure to an ototoxic substance, 3,3'-iminodiproprionitrile (IDPN) were first introduced in the rat (Seoane et al., 2001; Sedó-Cabezón et al., 2014, 2015; Martins-Lopes et al., 2019a) and more recently in the mouse (Greguske et al., 2019). Subchronic exposure to IDPN in drinking water at low doses allowed for progressive ototoxicity, leading to a partial and reversible loss of function. Although the subchronic IDPN protocol was shown to cause postural and locomotor deficits (Martins-Lopes et al., 2019a), its effects on the gaze stabilizing reflexes, namely the vestibulo-ocular and optokinetic reflexes, have not yet been described.

The primary objective of the present study is first to assess how subchronic exposure to IDPN may affect the function of the different vestibular endorgans. To that end, we took advantage

of our recently described methodology (Simon et al., 2020, 2021) using canal-specific and otolith-specific tests. Quantification of the vestibulo-ocular reflexes is a sensitive and specific method to assess the functionality of the sensory-motor vestibular pathway; it is the most used test in clinics, and highly correlates to quality-of-life reports in patients suffering from acute peripheral diseases (Möhwald et al., 2020).

The secondary objective is to determine whether visual substitution occurs following transient and partial vestibular loss. Optogenetic stimulation of the vestibular pathway demonstrated the recruitment of circuits involved in visual processing at the midbrain, thalamic and cortical regions (Leong et al., 2019). Recent imaging studies in rodents have shown that acute vestibular loss triggers brain-wide adaptive plasticity in circuits known to be involved in visual processing (Zwergal et al., 2016; Grosch et al., 2021). In addition, it was previously shown that OKR plasticity is triggered during vestibular compensation following a permanent vestibular lesion (Faulstich et al., 2006; Nelson et al., 2017).

We report that 6 weeks of IDPN subchronic treatment affects both the canal- and otolith-dependent vestibulo-ocular reflexes and that organ-specific loss of type I HC correlates with individual mice's impairments. We show that optokinetic adaptive compensation is frequency-specific and delayed with respect to the VOR changes. OKR changes occur at the frequencies where physiologically the vestibular inputs dominate visuo-vestibular gaze stabilization. We demonstrate that despite the functional recovery of their vestibulo-ocular reflexes, the visuo-vestibular integration remains impaired in some IDPN-treated mice. We suggest that the "noisiness" of the recovered vestibular signal affects their capacity to optimally combine visual and vestibular responses. Overall, these results shed light on the dynamic of multisensory reweighting in patients suffering from fluctuating peripheral vestibular malfunction.

Results

Effects of the subchronic treatment of IDPN on the canal- and otolith-dependent VOR.

To investigate the effects of the IDPN on vestibulo-ocular reflexes (VOR), animals were exposed to the ototoxic compound in the drinking water for six weeks (Treatment period), followed by 6 weeks of standard drinking water without IDPN (Washout period). The vestibulo-ocular reflexes were quantified every two weeks using canal-specific and otolith-specific tests. Horizontal sinusoidal rotations in the dark were performed and oculomotor responses were recorded using video-oculography (Figure 1A) to study the impact of IDPN treatment on the canal-dependent angular VOR (aVOR). Typical raw aVOR traces are shown in Figure 1B. At W6 the amplitude of the eye movements was distinctly reduced compared to W0, while at W12 the amplitude of the response appeared partially restored. The dynamics of decrease and recovery of the mean aVOR gain over the course of the protocol are reported in Figure 1C for both IDPN (n=21) and SHAM (n=22) groups. The evolution over time of the aVOR gain is significantly different for the two groups of mice (ANOVA Weeks x Group interaction, $F(6,246)=29,949$, $p<10^{-4}$). Before treatment, both groups responded similarly to the sinusoidal stimulations and their aVOR gain remained unchanged until 2 weeks of treatment (W2). However, starting W4 the aVOR gain of IDPN group significantly decreased with respect to W0 (Newman-Keuls post hoc test: IDPN W0 vs W4 $p<10^{-4}$) and was significantly lower compared with the SHAM group (W4, IDPN vs SHAM $p<10^{-4}$). The aVOR gain of the IDPN group remained lower compared to SHAM through the rest of the protocol (W6 IDPN vs SHAM $p<10^{-4.}$, W8 IDPN vs SHAM $p<10^{-4}$, W10 IDPN vs SHAM $p<10^{-4}$, W12 IDPN vs SHAM $p<10^{-4}$) with a minimum reached at W6 corresponding to ~2/3 of aVOR loss (IDPN W4 vs W6 $p<10^{-4}$, IDPN W6 vs W8 $p=0,043762$). At the end of the six weeks of washout, the mean aVOR significantly improved (IDPN W6 vs W12 $p<10^{-4}$) to levels observed at W4 (IDPN W4 vs W12 $p=0.561969$).

VOR gain decrease was paralleled with significant phase leads that affected all tested frequencies at week 6 (Supplementary Figure 1B, ANOVA repeated measures Weeks x Group Interactions $F(6, 246)=14.528$, $p<10^{-4}$). Overall, canalar responses remained unaffected until week 2, but the amplitude and/or timing of the aVOR was abnormal from week 4 until the

102 end of the protocol, despite a significant recovery of angular VOR responses observed during
103 the washout period.
104 To determine whether otolith-dependent VOR was also affected by IDPN treatment, ocular-
105 counter roll responses were tested during static lateral inclination in the range ±40° (OCR;
106 Figure 1D). Examples of raw traces and quantification of the response are shown in Figure 1E,
107 and mean gain of the OCR of each group is plotted in Figure 1F (n=13 IDPN, n=14 SHAM). The
108 modulations of responses amplitude were significantly different between IDPN and SHAM
109 groups (ANOVA repeated measures Weeks x Group Interaction $F(6, 150)= 7.7411$ $p<10^{-4}$). We
110 note that there was a significant difference between SHAM and IDPN during the initial
111 measurements at W0, before any treatment. However, at this timepoint mice were not yet
112 separated into different groups. This incidental difference completely disappeared on the
113 measurement performed at W2 (W2 IDPN vs SHAM p=0.8135). While the gain of the SHAM
114 group stays in a 0.5-0.6 range over the whole duration of the protocol, the responses of the
115 IDPN group significantly decreased at W4 compared to the SHAM group (W4 IDPN vs SHAM
116 $p<10^{-4}$). This decrease was larger at W6 (IDPN W4 vs W6 p=0.023) and stayed significantly
117 different from the SHAM group until W8. At W10 and W12, the OCR of IDPN group recovered
118 to a level comparable to the SHAM group (W10 IDPN vs SHAM p=0.1262, W12 IPDN vs SHAM
119 p=0.3385).
120 Sub-chronic treatment of IDPN was also investigated through the dynamic Off Vertical Axis
121 Rotation (OVAR) test (Supplementary Figure 1C), which primarily reflects maculo-ocular
122 (dominantly otolithic) responses integrated by central vestibular pathways. The maculo-
123 ocular reflex (MOR) bias decreased significantly compared to the SHAM group (ANOVA Weeks
124 x Group, $F(6, 132)= 10.076$, $p<10^{-4}$) starting W2 of treatment (W2 IDPN vs SHAM p=0.0018),
125 demonstrating that ototoxicity already affected the vestibular system at this early time point.
126 The maximal decrease was reached at W6 (W6 IDPN vs SHAM p=0.00012) and recovery led
127 to normal responses at W12 (W12 IDPN vs SHAM p=0.4709).
128
129 **Comparison of otolith- and canal-dependent plasticity in individuals.**
130 To compare the dynamic of canal- and otolith-dependent VOR alterations, the paired VOR
131 and OCR gains measured in individuals from the IDPN group (n=13) are plotted together
132 (Figure 2). Alteration in canal- and otolith-dependent responses followed a very similar time

133 course (OCR vs aVOR at 1HZ on figure 2A; similar patterns were obtained with the other tested
134 frequencies (not shown)).
135 To investigate further the organ-specific responses, the individual values of VOR gain at 1Hz
136 (left panel) and OCR slope (right panel) are plotted in Figure 2B. These plots show the
137 variability of the responses observed in different individuals. 2/3 of the mice had aVOR
138 responses lowered by more than 50%, while 1/3 had milder aVOR impairments. In most cases,
139 however, the aVOR gain decreased notably between W4 and W6 and started to recover from
140 W8 (compare individual slopes in Figure 2B). Similarly, OCR gains were variable between
141 individuals. However, the dynamic of the variations in otolith-dependent responses followed
142 a pattern comparable to that of the canal-dependent changes.
143 To determine whether the changes in canal- and otolith-dependent responses were
144 proportional, individual variations in gain since pre-treatment of the aVOR and OCR were
145 compared at W6 (Figure 2C) and W12 (Figure 2D). At W6, there was a significant correlation
146 between the amplitude of the changes observed in aVOR and OCR, such that canalar and
147 otolithic loss of function was proportional (slope of regression line: 0.5586). Despite the
148 general recovery, this significant correlation was preserved at W12: the recovery in canal-
149 dependent responses was proportional to the recovery in otolith-dependent responses (slope
150 of regression line: 0.5566). Overall, these results suggest that the subchronic IDPN treatment
151 similarly affects the vestibulo-ocular reflexes that depend on semi-circular canals and on the
152 otolithic organs, respectively.
153
154 **Effects of the IDPN exposure on the number of hair cells in the vestibular epithelia.**
155 To correlate the vestibular loss of function to the structural changes induced by the ototoxic
156 compound, vestibular epithelia were dissected and labelled to assess the number of hair cells
157 (HC) in the organs. One horizontal semi-circular canal and one utricule were harvested at W6
158 for n=7 IDPN and n=4 SHAM, and at W12 for n=8 IDPN and n=4 SHAM, and each organ
159 epithelium was divided into the central and peripheral region to differentiate the possible
160 participation of zone- and organ-specific HC to the vestibular function. Vestibular HC were
161 labelled with type-specific immunomarkers in both endorgans (Figure 3). Confocal
162 Immunostaining data are presented in Figure 3A1 for the horizontal semi-circular canals and
163 Figure 3B1 for the utricule. 6-week long treatment of IDPN exposure led to a significant
164 reduction in the labelling of type I HC in the canal crista (quantified in Figure 3A2, Non

165 parametric Kruskal-Wallis test, SHAM vs IDPN Spp1, p=0.0322; SHAM vs IDPN Caspr1,
166 p=0.0268; Supplementary Figure 2A1 and B1 for the peripheral zones) and in the otolith
167 macula (Figure 3B2, Non parametric Kruskal Wallis test SHAM vs IDPN Spp1, p=0.0279; SHAM
168 vs IDPN Caspr1, p=0.0343). However, the treatment did not alter type II HC-specific labelling
169 as the number of Calre+ cells in the IDPN group was similar to the SHAM in all regions of either
170 vestibular endorgans (Figure 3A2, canal crista, Calre: Non parametric Kruskal-Wallis test IDPN
171 vs SHAM, p>0.9999; Figure 3B2, otolith macula, Calre: SHAM vs IDPN, p>0.9999). Importantly,
172 the total number of HC marked with Myo7a (labelling both type I and type II HC) was not
173 significantly different between the IDPN-treated mice and the SHAM, suggesting that the
174 alteration of type I HC is not associated with cell loss. Moreover, at W12 the number of type
175 I HC labelled in the IDPN-treated mice was no longer significantly different from the SHAM
176 group in either endorgans (Figure 3A3 for crista; Figure 3B3 for macula). The count of type II-
177 specific markers and of non-specific HC markers was not statistically different between SHAM
178 and IDPN either, so that overall no difference persisted at W12, indicating a structural
179 recovery at the end of the washout period.
180 To determine how the loss of HC correlates with organ-specific functional tests, the numbers
181 of type I and II HC in the central region of the horizontal semi-circular canals are plotted as a
182 function of the mean aVOR gain for mice at W6 and W12 (Figure 3C1). Both markers of type I
183 HC (Caspr1 and Spp1, left panels) were significantly correlated with the aVOR gain (linear
184 regression, Spp1: r^2=0.5128, p=0.0001; Caspr1: r^2=0.4948, p=0.0002) whereas the rather
185 constant number of type II HC in the ampulla did not correlate with the variation observed in
186 aVOR function. Finally, to determine if the correlation was due to the recovery occurring
187 between W6 and W12, the number of CASPR+ cells of IDPN mice counted at W12 are plotted
188 as a function either of the individual aVOR gain at W12 (pink squares) or aVOR gain at W6
189 (black circles), paired by an arrow (Figure 3C2). The recovery of the vestibular function
190 between W6 and W12 induces a shift toward the W12 linear regression, reinforcing the
191 notion that the recovery of function was related to the increase in the number of hair cells
192 with normal expression of biochemical markers (Figures 3B3 & 3C2).
193 The numbers of type I HC and II HC found in the striolar region of the utricule are similarly
194 plotted in relation to the OCR gain (linear regression, Spp1: r^2=0.6011, p<0.0001; Caspr1:
195 r^2=0.6342, p<0.0001, Figure 3C3). Again, the otolithic function correlated with the number of
196 type I HC, and not type II HC in the central region. Furthermore, the correlation found

197 between the otolithic function and the number of type I HC related to the increase in the
198 number of hair cells after the recovery period (Figure 3C4). A similar correlation between
199 organ-specific function and the number of type I HC was also found in the peripheral regions
200 of these organs (see Supplementary Figure 2C1, C2 for the SCC, and Figure 2D1, D2 for the
201 utricule).
202 Taken together, comparison at W6 and W12 of non-specific HC and type I-specific HC markers
203 suggest that the ototoxic effect induces a transient biochemical alteration of type I HC rather
204 than a definitive hair cell degeneration. Overall, IDPN-induced alteration of canal and otolith
205 functions are correlated with the ototoxic effect on type I, and not type II, HC in the central
206 and peripheral zones of vestibular endorgans.
207
208 **Effects of the subchronic treatment of IDPN on the optokinetic reflex.**
209 To determine the effects of the subchronic treatment of IDPN on the optokinetic reflex, mice
210 were tested with sinusoidal rotations of a virtual drum (Figure 4A). An example of raw traces
211 of the evoked horizontal eye movements is shown in Figure 4B for different timepoints (0.5Hz
212 at 10deg.s^{-1} optokinetic stimulation). The mean OKR gain for all tested frequencies is plotted
213 in Figure 4C for SHAM (n=12) and IDPN-treated mice (n=12). The mean OKR gain of IDPN mice
214 was significantly different from the mean OKR gain of SHAM mice at W8 (interaction between
215 Weeks and Group F(6,132)=2.9845, p=0.0091; IDPN W0 vs W8, p=0.0216) where it reached
216 its peak (IDPN W0 vs W8, p=0.00037). The gain stayed significantly larger compared to the
217 SHAM until the end of the washout period (W12 IDPN vs SHAM, p=0.046).
218 To determine whether this OKR modulation was frequency-specific, the gain of the 5 tested
219 frequencies was compared for W0, W6, W8 and W12 (Figure 4D). There was at W0 no
220 difference between SHAM and IDPN mice (Figure 4D, left panel, W0). At W6, there was a
221 significant difference between the IDPN and SHAM groups limited to 0.5 and 1Hz (W6 IDPN
222 vs. SHAM, 0.5Hz, p=0.013117; W6 IDPN vs. SHAM, 1Hz, p<10^{-4}). At W8, all frequencies above
223 0.2Hz were significantly increased compared to the SHAM group (W8 IDPN vs. SHAM, 0.33Hz,
224 p=0.027687; 0.5Hz, p=0.0025; 1Hz, p=0.00015). At W12, the gain remained high for both 0.5
225 and 1Hz whereas the gain at 0.33Hz was no longer significantly larger than the SHAM group
226 (W12 IDPN vs. SHAM, 0.33Hz, ns; 0.5Hz, p=0.0069; 1Hz, p=0.00078). Globally, responses at
227 higher frequencies (0.33, 0.5 and 1 Hz) were significantly increased (ANOVA Weeks x Group x
228 Frequencies interaction, F(24, 528)=6.5870, p<10^{-4}) whereas responses at the lowest

229 frequencies (0.1 and 0.2Hz) were not significantly modulated. Additionally, these changes in
230 gain for frequencies >0.2Hz were not accompanied by changes in the timing (phase) of the
231 OKR (Figure 4E) (ANOVA, Weeks x Group x Frequencies interaction, p=0.3802).
232
233 **Relation between VOR decrease and optokinetic increase**
234 To correlate the changes in vestibular pathway with the frequency-specific changes observed
235 in the optokinetic pathway, we compared the responses in aVOR and OKR obtained at the
236 frequencies that were common between the 2 tests (i.e 0.2 Hz, 0.5 Hz and 1Hz) for n=12 SHAM
237 and n=12 IDPN treated mice by comparing the increase in the OKR and decrease in VOR
238 relative to W0 (Δmean gain, see Figure 5). To determine whether the changes in VOR and OKR
239 were proportional, we compared the paired decrease and increase in the mean ΔaVOR and
240 ΔOKR gain after 8 weeks of treatment, when the difference between the 2 reflexes peaked
241 (Figure 5A). The vast majority (n=11/12) of IDPN-treated mice showed a decrease in aVOR
242 and an increase in OKR (top left quadrant corner, Figure 5B), which was not the case for SHAM
243 mice (blue squares). However, there was no correlation between the amplitude of the VOR
244 decrease and the amplitude of the OKR increase, i.e mice that had the greatest VOR loss did
245 not show the largest OKR increase (slope in the regression line: 0.27, p=0.0834).
246 To determine whether the parallel changes in OKR and VOR are frequency-specific, Figure 5C
247 compares the gains measured at W0 and W8 for each frequency. At 0.2Hz, there was a
248 significant decrease in aVOR (IDPN W0 vs. W8 0.2Hz $p<10^{-4}$), however the OKR was not
249 modified. On the other hand, at 0.5 and 1 Hz significant VOR decreases (IDPN W0 vs. W8,
250 0.5Hz, $p<10^{-4}$; 1Hz, $p<10^{-4}$) were accompanied by a significant OKR increase (IDPN W0 vs. W8,
251 0.5Hz, $p<10^{-4}$; 1Hz, $p<10^{-4}$). To examine this frequency-selective increase, the percentage of
252 change in the OKR gain is plotted as a function of the *vestibular weight*, determined as the
253 ratio between the aVOR and aVOR+OKR values at week 0. The *vestibular weight* therefore
254 represents the frequency-dependent relative influence of the vestibular signal on gaze
255 stabilization. Figure 5D shows that at week 8, the change in the OKR occurred at the
256 frequencies for which the *vestibular weight* is dominant (>50%), and that the increase in OKR
257 was positively correlated with the *vestibular weight* among frequencies (slope of the
258 regression line: 1.235, $r^2=0.6299$, p<0.0001). Overall, these results suggest that the increase
259 in OKR gain observed at high frequencies could correspond to a "visual substitution" occurring
260 primarily in the range where the vestibular inputs are normally dominating gaze stabilization.

261 **Visuo-vestibular interactions following alteration of vestibular inputs**

262 To investigate whether OKR increase did constitute a "visual substitution" that maintained
263 optimal gaze stabilization at light despite vestibular loss, we investigated how IDPN-treated
264 mice integrated vestibular and visual inputs. To this end, a session of combined visual and
265 vestibular stimulation (aVOR in light, here referred as *Combined Gaze Response* or CGR
266 condition) was performed at W6 and at W12 (n=19 IDPN; n=12 SHAM). A model (see methods)
267 was implemented to predict the theoretical CGR (visuo-vestibular) gain and phase from aVOR
268 and OKR (unimodal) measured values. The model was first optimized to correctly predict the
269 average SHAM CGR gains and phases (Figure 6A) from their individual aVOR and OKR
270 responses, and then applied to the individual IDPN. The predicted and observed CGR gain
271 (Model factor) were compared for each treatment group (ANOVA Group x Model, $F(1,29)=$
272 12.236, $p=0.0013$): as expected, model predictions for SHAM well-matched experimental data
273 (Post-hoc Newman-keuls, SHAM MODEL vs SHAM CGR, $p=0.41$). When applied to IDPN mice
274 the model predicted that their CGR gain should be lower compared to SHAM (shaded blue
275 and red areas on Figures 6A and 6B, Post-hoc Newman-keuls, SHAM MODEL vs IDPN MODEL,
276 $p=0.00176$), suggesting that even an optimal combination of unimodal responses could not
277 restore completely normal CGR in IDPN-treated mice. The CGR gains observed for IDPN-
278 treated mice actually revealed how their visuo-vestibular responses were not only reduced
279 compared to SHAM (compare solid blue and red lines in Figure 6A-B, Post-hoc Newman-keuls,
280 SHAM CGR vs IDPN CGR, $p=0.00055$), but were even inferior to the prediction of the model
281 (compare solid red line and shaded red area in Figure 6B, Post-hoc Newman-keuls, IDPN
282 MODEL vs IDPN CGR, $p=0.00041$). This suggests that the IDPN-treated mice sub-optimally
283 combined their residual/compensated vestibular and visual reflexes to stabilize gaze. Figure
284 6C illustrates the relationship between the measured CGR gain and the prediction of the
285 model for all tested frequencies. For SHAM animals, CGR gain values were positioned along
286 the unity line that represents a close match between predicted and measured CGR
287 (mean±SEM: SHAM MODEL 0.8255±0.053; SHAM CGR 0.8375±0.042). For IDPN-treated mice,
288 the responses formed 2 subgroups that did not correspond to different frequencies (all
289 frequencies found in either subgroup). The first subgroup was intermingled with the SHAM
290 responses, with measured CGR values slightly lower than predicted values (MODEL
291 0.7457±0.028; CGR 0.6644±0.052). The second subgroup represented mice for which the
292 measured CGR significantly underperformed the predicted CGR (MODEL 0.4685±0.022; CGR

293 0.2005±0.01). To investigate the difference between the two subgroups, the VOR, OKR and
294 CGR values were plotted for the n=19 IDPN mice (Figure 6D). A hierarchical cluster analysis
295 (see methods) suggested the presence of two main clusters (see dendrogram in Figure 6D).
296 The first cluster (Δ+, n=12; in green in Figure 6D, E, and F) comprised individuals with CGR
297 values higher than OKR (positive values on Δ=CGR-OKR), i.e with gaze stabilization at light
298 better in the presence of vestibular stimulation. The second cluster (Δ-, n=7; depicted in
299 orange) is composed of individuals with low CGR (<0.4). IDPN mice from the Δ- cluster have
300 degraded responses during bimodal visuo-vestibular stimulation compared to unimodal OKR
301 stimulation (negative value of Δ indicates CGR responses lower than OKR responses). Notably,
302 this degraded CGR is not solely a consequence of a low VOR gain, as some Δ+ mice identified
303 by the second differentiation of the clustering analyses (depicted with grey diamond symbols
304 in Figure 6D, and indicated as $\Delta+_{(-)}$) also showed low unimodal VOR gain responses.
305 We reasoned that the worsening of the gaze responses in the bimodal condition compared
306 to the OKR-only condition could be a consequence of a poorly reliable, noisy vestibular signal.
307 Based on a cycle-to-cycle sweep analysis, two additional features of the VOR responses were
308 quantified (see methods): the mean amplitude of the raw sweep during VOR stimulation and
309 the VOR response reproducibility between sweeps. The mean VOR raw sweep amplitude
310 could not statistically differentiate Δ- and $\Delta+_{(-)}$ mice (Figure 6E, orange triangle vs green
311 diamonds p=0.0857), suggesting that vestibular signal of comparable amplitude improved or
312 deteriorated the CGR response in the $\Delta+_{(-)}$ and Δ- mice, respectively. On the other hand, the
313 VOR reproducibility clearly discriminated Δ- and $\Delta+_{(-)}$ mice (Figure 6F, orange triangle vs green
314 diamonds, p=0.0001). There was a strong correlation between the inter-sweep reproducibility
315 and the capacity of the mice to stabilize gaze in presence of vestibular inputs at light. This
316 result suggests that the incapacity of the Δ- group to compute optokinetic signals in the
317 presence of vestibular stimulation could relate to the poor reliability of the vestibular signal.
318 Overall, these data suggest that in some situations the presence of a degraded vestibular
319 signal of significant amplitude (panel 6E) but poorly reliable (panel 6F) can be detrimental to
320 properly stabilize gaze in presence of visual and vestibular inputs.

321 Discussion

322 **IDPN as a model of partial and transitory loss of vestibular function**

323 IDPN has long been established as an ototoxic compound targeting vestibular HC in the
324 different vestibular endorgans of rats (Llorens et al., 1993, 1994; Llorens and Demêmes, 1994)
325 and later in guinea-pig, frogs and mice (Soler-Martin et al., 2006; Greguske et al., 2019). Its
326 ototoxic vestibular effects were used as a tool to study extraocular muscle development
327 (Brueckner et al., 1999) or more recently to induce permanent vestibular loss in mice (Yang
328 et al., 2019; Zeng et al., 2020) and study hair cell regeneration (Sayyid et al., 2019). The sub-
329 chronic, reversible protocol used in our study was validated previously in rats (Sedó-Cabezón
330 et al., 2015; Martins-Lopes et al., 2019b; Maroto et al., 2021) and mice (Boadas-Vaello et al.,
331 2017; Greguske et al., 2019) with postural/locomotor quantification of vestibular loss. We for
332 the first time demonstrate that the subchronic protocol leads to a progressive and reversible
333 loss of vestibulo-ocular reflexes. These previous studies further demonstrated some of the
334 cellular mechanisms associated with the progressive loss of postural control: ototoxic effects
335 lead to the early dismantlement of calyceal junction, followed by synaptic uncoupling, both
336 of which were shown to be reversible, while continuation of the IDPN treatment would lead
337 to hair cell extrusion and long-term, permanent lesion. Hair cell loss was also demonstrated
338 to occur in a central to peripheral order within vestibular epithelia, and in crista to utricule to
339 saccule order (see Sedó-Cabezon et al. 2015). Greguske et al. (2019) convincingly
340 demonstrated that type I HC show greater sensitivity than type II HC to IDPN subchronic
341 exposure (Maroto et al. 2021). Given these data, a primary goal of the present study was to
342 try to correlate the loss of VOR functions to organ-specific, zone-specific, and cell-type-
343 specific effects.
344 Loss and substantial recovery of the vestibular function quantified by VOR measures were
345 found to be correlated with the number of type I HC in both canals and otoliths. A parallel
346 was previously established between hair cell integrity and VOR following ototoxic protocols
347 in mice (Cassel et al., 2019; Yang et al., 2019; Zeng et al., 2020), but these were established at
348 the population level. Here, we for the first time specifically correlated the loss of hair cells
349 and loss of VOR function both at the individual level and in an organ-specific way. aVOR and
350 OCR tests demonstrated a parallel decrease in canal- and otolith-dependent functions,
351 respectively. The 6 week-long treatment was followed by a 6 week-washout period, allowing
352 a significant but partial recovery of the aVOR, and complete recovery of the OCR. The
353 individual correlations between these functional tests and the number of hair cells counted
354 in the ampullae and maculae of the mice were found to be particularly significant, both during

355 the trough (W6) of VOR function and after the recovery period (W12) (Figure 3C,). We,
356 however, did not find any difference between the hair cell loss in the central vs. peripheral
357 zones of the organs, and can therefore not conclude on any putatively differential implication
358 of these areas in the VORs. Overall, these organ-specific structure-function correlations
359 confirm that the vestibulo-ocular reflex can serve as a proxy indicating the status of the
360 vestibular endorgans. It further validates the use of the aVOR and OCR as relevant tests
361 reflecting hair cell integrity at the level of the ampullae and maculae, respectively.
362
363 **Differential alteration of type I versus type II hair cells**
364 The subchronic treatment affected type I HC more than type II HC, in accordance with
365 previous reports (Llorens et al. 1993; Maroto et al. 2021). Susceptibility to IDPN was also
366 reported to vary between different mouse strains (Boadas-Vaello et al., 2017; Wilkerson et
367 al., 2018). Interestingly, we used a different strain of mice than the one used in a previous
368 subchronic experiment (Greguske et al. 2019) and have not observed any type II hair cell loss
369 either, nor differences between males and females (data not shown).
370 Hence, IDPN treatment induces a loss of cell markers specific to type I HC, with no effects on
371 type II markers. Two types of markers were used to identify type I HC. Spp1 targeted a protein
372 located on the neck of the hair cell (McInturff et al., 2018), while Caspr1 is located at the
373 calyceal junction of the afferent terminal, and has been proven to be necessary for the
374 functionality of the synapse between the hair cell and its connected afferent (Sousa et al.,
375 2009). Though it is not possible to compare for one individual the number of cells before and
376 after treatment, the number of cells labelled for either of these proteins decreased
377 significantly compared to SHAM group, whose numbers are consistent between W6 and W12.
378 The loss of Caspr1 marker induced by IDPN sub-chronic treatment has been linked to hair cell
379 detachment from the calyx terminal and loss of vestibulo-spinal reflexes, and both Caspr1
380 expression and vestibular function recover during washout (Sedó-Cabezón et al., 2015;
381 Greguske et al., 2019; Maroto et al., 2021). Only after a longer IDPN exposure does hair cell
382 extrusion occur, associated with persistent functional deficits. In theory, the loss of vestibular
383 function observed in both canal- and otolith-dependent VOR at W6 could be linked to loss of
384 type I HC. In adult rodents, however, the regeneration of hair cells leads to the formation of
385 cells with type II HC features (González-Calvo et al., 2021), so the recovery of type I cellular
386 markers at W12 is likely not a result of cell regeneration. Also, the apparent dramatic loss of

387 Caspr1 and Spp1 HC (90%) at W6 was in contrast with the much smaller and not significant
388 loss in Myo7a cells (29%), supporting the conclusion that the sensory cells persisted in the
389 epithelium despite Caspr1 loss, and that the recovery in the number of type I HC observed at
390 W12 was more likely the result of molecular repair, not cell regeneration. In addition, we
391 observed a similar loss of Spp1 marker at W6, normally located in the neck of the hair cell. As
392 such the loss of vestibular function could rather be attributed to a global disorganization of
393 the synapse and defective hair cell function, associated with a transitory large decrease of the
394 Spp1 and CASPR1 proteins and a smaller decrease in Myo7a. In accordance with this
395 hypothesis, the number of Spp1 and Caspr1 positive cells after the washout period at W12
396 was not significantly different from the SHAM group and correlated to the recovery of the
397 vestibular function observed at W12 for the IDPN mice (Figure 3C2). The altered expression
398 of proteins in type I HC induced by the sub-chronic treatment of IDPN seems to be reversible
399 in most individuals. One possibility is that definitive extrusion of type I HC occurred in the
400 most susceptible individuals that did not show recovery after the end of treatment. This in
401 fact was the case in the 2 individuals tested at W12 with immuno-histochemistry: CASPR
402 mean value (±S.E.M) of 18.5±5.5 compared to 34.5±4.359 for IDPN with recovery and
403 41.75±1.215 for SHAM). It was previously reported in the pigeon that type I HC and calyx
404 afferents take longer (12 weeks) to regenerate following aminoglycoside toxicity, while type
405 II and boutons endings regenerated in a week (Zakir and Dickman, 2006). Similarly, recovered
406 innervation for type I HC was delayed compared to type II HC in mice (Kim et al., 2022). A
407 longer recovery period could be investigated in the case of the severely-affected mice to
408 confirm the absence of recovery in the longer term.
409
410 **Evidence for the role of type I hair cells in the vestibulo-ocular pathways**
411 To our knowledge, the direct implication of type I and type II HC in the VOR was never directly
412 tested. Type I and type II HC differ by many features, including their anatomical location
413 within the epithelium, electrophysiological properties, morphology and innervation by
414 afferents (Eatock and Songer, 2011). Seemingly, irregular afferents have been described as
415 predominantly innervating the central area and striolar zones of the ampullae and maculae
416 with calyx and dimorphic synaptic contacts, while regular afferents make dimorphic and
417 buttons contacts predominantly within the peripheral zones of cristae and extrastriolar zones
418 of maculae (Goldberg, 2000; Eatock and Songer, 2011; Contini et al., 2022).

419 Functionally, regular afferents recorded in the monkey show a lower detection threshold than
420 irregular afferents (Sadeghi et al., 2007), while irregular afferents show higher gains and
421 phase leads (mouse: Lasker et al., 2008; Cullen, 2019), and would be better optimized for
422 encoding high dynamic stimuli (Cullen, 2019). Seminal studies have suggested that irregular
423 afferents would constitute ~1/3 of the excitatory drive received by central neurons
424 responsible for the VOR (Highstein et al., 1987; Boyle et al., 1991), and functional ablation
425 targeting irregular afferents that VOR might function normally with only regular afferent
426 inputs (Minor and Goldberg, 1991).
427 Based on these data, it would be tempting to infer that only the most regular and tonic
428 elements of the vestibular periphery are responsible for the VOR. However, the
429 correspondence between hair cell properties and afferents properties is only partial, such
430 that the two phasic/irregular and tonic/regular channels for head motion signals are
431 constituted of both types of hair cells and afferents (Eatock and Songer 2011; Beraneck and
432 Straka, 2011). It has also been recently shown that both types of hair cells contribute to
433 vestibular evoked potential responses, previously described as mostly type I-specific (Sayyid
434 et al, 2019). Our data further contradict such a simplified scheme as the VOR is severely
435 affected by the specific loss of type I HC in both central and peripheral parts of the vestibular
436 endorgans. Carey and colleagues (1996) previously reported a better correlation of VOR
437 recovery with type I than with type II HC following ototoxic lesions in the chick. Overall, the
438 result of ototoxic studies, including the present one, demonstrate a fundamental role of type
439 I HC in the encoding of vestibular signals that drive the vestibulo-ocular reflexes, even in the
440 relatively low range (Carriot et al., 2017) of head movements tested. Our results are
441 compatible with the hypothesis of a convergence of heterogeneous peripheral neural
442 elements at the level of central vestibular nuclei, where intrinsic properties of central
443 vestibular neurons (Straka et al., 2005; Beraneck and Idoux, 2012) supplemented by network
444 properties (Beraneck et al., 2007; Pfanzelt et al., 2008; Beraneck and Straka, 2011) would
445 differentially integrate vestibular signals further processed in the different vestibular
446 pathways (Sadeghi and Beraneck, 2020).
447
448 **Visuo-vestibular interactions after IDPN treatment**
449 OKR plasticity following vestibular loss concerned gain, and not phase, modifications for
450 frequencies >0.33Hz. Previous studies have reported an increase in OKR gain following a

451 permanent vestibular lesion for a non-specific range of frequencies (Shinder et al., 2005;
452 Faulstich et al., 2006; Nelson et al., 2017). One key to understand the frequency-specific OKR
453 plasticity could be the physiological dominance of vestibular inputs in the gaze stabilization
454 process at high frequencies (Faulstich et al., 2004). The visual inputs could be reweighted and
455 potentiated specifically in the range where the vestibular loss has the most impact on gaze
456 stabilization (Figure 5D).
457 The VOR and OKR work synergistically to stabilize gaze by compensating for head and visual
458 surround movements, respectively (França de Barros et al., 2020). If the reflexive eye
459 movements are not perfectly compensatory, an error signal (e.g retinal slip) is produced that
460 drives adaptation of the VOR (Boyden et al., 2004; Dean and Porrill, 2014; Shin et al., 2014)
461 and OKR (Glasauer, 2007; Kodama and du Lac, 2016). In an effort to understand the
462 integration of VOR and OKR, Holland and colleagues (2020) recently proposed that OKR would
463 account for the retinal slip not compensated by VOR. Within that framework, the changes in
464 the OKR could happen preferentially as a function of the vestibular weight, i.e in the range of
465 movements where the loss of vestibular inputs generates the largest retinal slip. While
466 present data are evidence for frequency-specific adaptation, how this relates to alteration in
467 vestibular inputs and/or visual feedback signals remains to be determined.
468 The increase in OKR gain could be seen as a substitution for the decrease in the VOR. However,
469 even after VOR recovery, the optimal integration of OKR and VOR (as predicted by our
470 MODEL) led to a degraded combined gaze response (CGR) with respect to SHAM mice. Even
471 worse, the measured CGR was inferior to the predicted CGR (Figure 6B). This observation
472 suggests that the integration of visual and vestibular signals during CGR is more than a mere
473 summation of the gain and phase of the 2 unimodal reflexes, but is also affected by other
474 factors. In fact, a subset of the IDPN individuals showed severely degraded bimodal
475 responses, so that their combination of VOR and OKR is not only sub-optimal but also less
476 effective than the unimodal (OKR) reflex. A sweep-based analysis suggested that in these
477 individuals, the VOR unimodal responses were not reliable, i.e the low reproducibility
478 indicates that the same stimuli are unfaithfully encoded into eye movements. We interpret
479 this low reproducibility as a sign of noisiness within the VOR pathway that would not only
480 preclude the optimal integration of both sensory signals, but also disturb the use of retinal
481 information to stabilize the gaze. According to statistical optimality theories, as the Maximum
482 Likelihood principle, the decrease in VOR reliability should lead to a reduction in its relative

483 sensory weight. This filtering-out of a degraded signal has been shown during visuo-vestibular
484 integration for monkey heading perception (Fetsch et al., 2010), or for human object
485 discrimination using visual and haptic senses (Ernst and Banks, 2002).Our results suggest that
486 the gaze stabilizing system is not able to optimally adapt to the degradation by filtering-out
487 vestibular signals during combined visuo-vestibular combination.
488 The integration of visual and vestibular inputs occurs in several structures, including in the
489 cerebellar flocculi (Jang et al., 2020) and brainstem (Carcaud et al., 2017) (see review De
490 Zeeuw et al., 2021). In the case of vestibular loss, most of the defects are expected to concern
491 the central vestibular neurons involved in the VOR, which also integrate visual inputs (ES, or
492 eye-sensitive neurons; Beraneck and Cullen, 2007). After unilateral neurectomy, vestibular
493 neurons in the Deiters nuclei responded to higher frequencies during visual stimulation (Cat:
494 Zennou-Azogui et al., 1994), a change compatible with the hypothesis that OKR gain increase
495 partly takes place in the vestibular nuclei. It was shown that inhibitory floccular inputs (part
496 of the OKR indirect pathway) and excitatory vestibular inputs often colocalized on the
497 dendrites of central vestibular neurons. One possibility is therefore that the massive
498 disorganization of vestibular periphery inputs led in the long term to synaptic and intrinsic
499 changes at the level of central vestibular neurons (Beraneck and Idoux 2012; Carcaud et al.
500 2017), thus impairing their capacity to optimally integrate both signals.

Material & Methods

Ethics

A total of 56 C57/BL6J mice in an equal partition of males and females were used for the protocol. Animals were used in accordance with the European Communities Council Directive 2010/63/EU. All efforts were made to minimize suffering and reduce the number of animals included in this study. All procedures were approved by the ethical committee for animal research of the Université Paris Cité.

Headpost implantation surgery and animal care

Surgical procedures, postoperative care, device fixation and animal surveillance during the protocol were performed as described previously in França de Barros et al., 2019, 2020. Briefly, mice anaesthetized with isoflurane gas had their heads shaved with small clippers. Then, lidocaine hydrochloride (2%; 2mg/Kg) was injected locally before a longitudinal incision of 1.5 cm was made to expose the skull. Just anterior to the lambda landmark, a small custom-built headpost (3x3x5mm; poly lactic acid) was cemented (C&B Metabond; Parkell Inc., Edgewood, NY) and laterally covered with resin (Heraeus) for protection. Animals were fully recovered 30 min after the end of the surgery, yet buprenorphine (0.05mg/kg) was provided for postoperative analgesia and they were closely monitored for the following 48 hours.

Subchronic ototoxic exposure

28 mice were treated with 3,3'-iminodiproprionitrile (IDPN, Sigma Aldrich, 317306, 90%) for 6 weeks (IDPN group) at 30mM concentration of IDPN in their drinking water. After 6 weeks of treatment, a washout period of 6 weeks followed. Previous experiments (Greguske et al., 2021) had demonstrated that at these concentrations, ototoxic lesions produced by IDPN are reversible. The SHAM group was tested the exact same way but was not exposed to IDPN in their drinking water. Video-oculography tests were performed before the beginning of the treatment and once every two weeks until week 12 (W12), for a total of 7 sessions of tests for each mouse.

Experimental groups

3 different batches of mice were used, each composed of both IDPN-treated mice and SHAM. The mice of the first one (n=19) were subjected only to vestibular stimulations, to test the

533 effect of IDPN on the canal-related or otolith-related VOR responses during the 12 weeks of
534 protocol. The second group (n=24), designed to compare the dynamic of VOR and OKR
535 changes was tested with angular VOR stimulations, otolithic test, optokinetic (visual)
536 stimulations, and combined vestibular and visual stimulation (VOR in light; referred to as
537 Combined Gaze Response or CGR). The third group (n=11) designed to correlate ototoxic
538 effects of IDPN on vestibular hair cells (HC) and VOR function was tested for canal-related or
539 otolith-related VOR responses, before treatment and after 6 weeks of treatment and
540 immediately used for immunohistochemical assessment of the vestibular sensory epithelia
541 (see below). A subset of the second group (n=12 out of 24) was also used for
542 immunohistochemical assessment at the end of the 12 weeks of protocol.
543
544 **Video oculography recording sessions**
545 The recording procedure was similar to the one presented in Carcaud et al. 2017 & França de
546 Barros et al. 2020. The animals were head-fixed in a custom build Plexiglas tube, and their
547 head was oriented in a 30° nose down position to align the horizontal canals to the yaw plane.
548 Their left eye movements were recorded using a non-invasive video oculography system (ETL
549 -200 Iscan, acquisition rate 120Hz, Stahl et al 2000). Eye, head, and virtual drum (OKR
550 stimulation) position signals were digitally recorded (CED mk3 power 1401, acquisition rate
551 1kHz) with Spike 2 software. Signals were analysed offline in Matlab (Matlab, the MathWorks,
552 Natick, MA, USA; RRID, SCR:001622) programming environment. The restraining apparatus
553 was fixed on a rotation platform on top of an extended rig with a servo-controlled motor.
554 Single VOR or OKR recording sessions lasted no longer than 45 minutes in total.
555
556 **Vestibular stimulations and analysis**
557 All vestibular-specific tests were performed in a temperature-controlled room with all sources
558 of light turned off except for computer screens. The turntable was further surrounded with a
559 closed box to isolate the animal from remaining light, with a final luminance inside the box
560 <0.02 lux. Myosis was induced with topical 2% pilocarpine applied 10 minutes before
561 experimentation.
562 *Vestibulo ocular reflex in dark (VORd) tests* were performed in the dark with the mouse
563 surrounded by an opaque black dome (Fig1.A). Sinusoidal angular rotations around the

564 vertical axis were used to record the horizontal angular vestibulo-ocular reflex (aVOR), at
565 different frequencies: 0.2, 0.5, 0.8; 1 and 2Hz at a peak velocity of 30°/s.
566
567 *Angular vestibulo-ocular reflex* analysis was similar to the one described in Carcaud et al.
568 2017. Segments of data with saccades were excluded from VOR slow-phase analysis. For
569 horizontal sinusoidal rotations, at least 10 cycles were analyzed for each frequency. VOR gain
570 and phase were determined by the least-squares optimization of the equation:
571
572 $$EH_v(t) = g \cdot \{[HH_v \cdot (t - t_d)] + \mathrm{C^{te}}\}$$
573
574 where EHv(t) is eye horizontal velocity, g (gain) is a constant value, HHv (t) is head horizontal
575 velocity, td is the dynamic lag time (in msec) of the eye movement with respect to the head
576 movement, and Cte is an offset. The td was used to calculate the corresponding phase (ϕ°) of
577 eye velocity relative to head velocity. The Variance-Accounted-For (VAF) of each fit was
578 computed as
579 $$1 - \left[\frac{var(est - EHv)}{var(EHv)}\right]$$
580
581 where *var* represents variance, *est* represents the modeled eye velocity, and *EHv* represents
582 the actual eye horizontal velocity. VAF values for VOR measures were typically between 0.70
583 – 1 (>95% of recordings), where a VAF of 1 indicates a perfect fit to the data. For IDPN-treated
584 mice, abnormally low (<0.15) values of gain associated with VAF<0.5 were nevertheless
585 included in the analysis but specifically reported in grey (Figure 2 & Supplementary Figure 1).
586
587 *Static Ocular Counter-roll reflex tests* were performed as described in (Simon et al., 2021) by
588 measuring the vertical eye movement generated in response to different roll angles. The table
589 was moved from left to right in incremental steps of 10° (from 0 to 40°), with static periods of
590 at least 10s between oscillations (Fig1.D) to record the stabilized eye elevation and
591 declination. The OCR gain corresponds to the slope of the linear regression of the vertical eye
592 angle *vs.* the head tilt angles (Oommen and Stahl, 2008).
593 *Off vertical axis rotation (OVAR) tests* were performed with the vestibular turntable tilted with
594 a 17° off-axis angle following the methodology described in Beraneck et al., 2012 & Idoux et

595 al., 2018. 50°/s continuous stimulations were performed in a counter-clockwise and then
596 clockwise direction. OVAR generates a continuous change in the head tilt angle, compensated
597 through a maculo-ocular reflex (MOR) by the generation of a horizontal nystagmus
598 compensating for the table constant rotation. This oculomotor response was quantified
599 following the methodology described in Idoux et al 2018. First, quick-phases were identified
600 and removed. During rotations, the velocity of horizontal slow phases is modulated
601 (modulation, μ) around a constant bias (β). Both parameters (μ and β) were calculated from
602 the sinusoidal fit of eye horizontal slow-phase velocity using the least-squares optimization
603 of the equation:

604 $$SP(t) = \beta + \mu \cdot sin[2\pi \cdot f_0 \cdot (t + t_d)]$$

605

606 where SP(t) is slow-phase velocity, β is the steady-state bias slow phase velocity, μ is the
607 modulation of eye velocity, f_0 is the frequency of table rotation, t_d is the dynamic lag time (in
608 msec) of the eye movement with respect to the head movement. The bias (Maculo-ocular
609 reflex Bias) is reported here as the main index of the MOR response (Hess and Dieringer, 1990;
610 Beraneck et al., 2012).

611

612 **Optokinetic reflex tests and analysis**

613 Horizontal optokinetic stimulations were performed as previously described in França de
614 Barros et al. 2020. The mice were placed under a semi-opaque plastic dome and all sources
615 of light were turned off. The projected stimulation consisted of a randomly distributed white
616 dots pattern on a black background image (250000 white dots, max width 0.075°). The
617 optokinetic sinusoidal stimulations were tested at 0.1, 0.2, 0.33, 0.5 and 1Hz at a peak velocity
618 of 10°/s. The gain and phase were obtained by the same least-squares optimization method
619 described above for the aVOR. To prevent putative cross effects between visual and vestibular
620 stimulations, VOR and OKR test sessions were performed on separate days.

621

622 **Combined visual and vestibular stimulations**

623 Combined visual and vestibular stimulations measuring the combined gaze reflex (CGR)
624 consisted of horizontal vestibular stimulations while projecting the fixed dotted pattern used
625 for OKR on the surrounding dome. Horizontal angular sinusoidal rotations were performed at
626 frequencies of 0.2, 0.5 and 1Hz with a peak velocity of 30°/s. The CGR gain and phase

627 quantifications were performed following the same methodology as for aVOR. To avoid
628 interference, these were performed on n=8 SHAM and n=12 IDPN after the end of the VOR
629 and OKR test sessions on W12. To test the effects at W6, a specific group of mice (n= 4 SHAM
630 and n=7 IDPN) was tested at W0 and W6.
631 A simple model has been developed to predict for each individual and for three stimulation
632 frequencies (0.2, 0.5 and 1Hz) the theoretical CGR response gain and phase were given the
633 same two parameters observed for their unimodal VOR and OKR responses. The experimental
634 VOR and OKR gain and phase are used to compute the sinusoid representing the two
635 unimodal responses. The gain and phase of the CGR sinusoid resulting from adding the VOR
636 and OKR sinusoids are quantified by measuring its peak-to-peak amplitude and by identifying
637 the time-lag that maximizes its cross-correlation with the sinusoidal stimulus (note that the
638 sum of two sinusoids with the same period, even if with different phases, is always a sinusoid).
639 Independently of the mouse, the unimodal VOR and OKR sinusoids are shifted in time before
640 their summation, in order to improve, on average, the fit between predicted and observed
641 CGR responses for SHAM mice. The two optimal shift parameters, one for VOR and one for
642 OKR, obtained for each frequency, are then used also for all IDPN-treated mice.
643 To identify subpopulations of IDPN-treated mice, we computed an agglomerative hierarchical
644 cluster tree on a dataset composed of individual aVOR gain and Δ (calculated as CGR-OKR
645 gain). The classification method used unweighted average Euclidean distance between
646 clusters.
647 To describe the mice VOR responses without any assumption about their sinusoidal nature
648 the two following characteristics have been quantified: the reproducibility of the ocular
649 response to the vestibular stimulation and the amplitude of the raw eye movements
650 generated by the vestibular stimulation. These analyses were performed on the slow phases
651 horizontal eye trajectories, *EHp(t)*, recorded during each sweep of stimulation.
652 The reproducibility index, *Rep*, was obtained by computing the matrix of correlation
653 coefficient, $R_{i,j}$, between each couple (*i,j*), of the *N* selected sweeps, and then computing the
654 mean of all above-diagonal elements of the matrix as reported in the following equation (this
655 choice aims at considering only once each $R_{i,j}$, since $R_{j,i}=R_{i,j}$ and to exclude diagonal elements,
656 $R_{i,i}=1$).

657 $$Rep = \frac{\sum_{i=1}^{N-1}\sum_{j=i+1}^{N} R_{i,j}}{N(N-1)/2}$$

658 The amplitude, *Amp*, of the raw eye movements was quantified by computing for each sweep
659 how much on average, during a stimulation cycle, the eye moved horizontally away from its
660 average position (σ_{EHp}). Before averaging this parameter over all the sweep, it had to be
661 squared. Finally, to have a parameter value in degrees, the root mean squared of the mean
662 was computed.

663 $$Amp = \sqrt{\frac{\sum_{i=1}^{N} \sigma_{EHp}^2}{N}}$$

664

665 **Immunolabelling of the hair cells**

666 Two groups of mice (n=11 at W6 and n=12 at W12) were used to perform
667 immunofluorescence analysis on hair cells in the vestibular endorgans. Mice were
668 anaesthetized with an overdose of intraperitoneal injection of ketamine hydrochloride
669 (10%)/xylazine (5%) and decapitated. The histology was done following the protocol
670 described in Maroto et al., 2021. The vestibular epithelia (one horizontal canal and one
671 utricule) were dissected and fixed for 1h in a 4% solution of paraformaldehyde (PFA). PFA was
672 washed twice with phosphate-buffered saline (PBS) and the samples were then embedded in
673 a cryoprotective solution (34.5% glycerol, 30% ethylene glycol, 20% PBS, 15.5% distilled
674 water) to be stored at -20°. Before the immunochemistry, samples were put at room
675 temperature and rinsed twice in PBS. While under slow agitation, the samples were incubated
676 twice, first for 1h with a 4% Triton X-100 (Sigma Aldrich) in PBS to permeabilise and a second
677 time for 1h in 0.5% Triton X-100 1% fish gelatin (CAS #9000-70-8, Sigma-Aldrich) in PBS to
678 block. The incubation with the primary antibodies was then performed in 0.1M Triton X-100,
679 1% fish gelatin in PBS at 4° for 24h. After rinsing, the second antibodies were incubated in the
680 same conditions. The 2nd antibodies were rinsed and the vestibular epithelia were mounted
681 on slides with fluoromount (F4680, Sigma-Aldrich) and were visualised with a confocal
682 microscope Zeiss LSM880 (with an objective of 63x NA:1.4). To properly analyse the whole
683 vestibular epithelium, Z-stacks of 0.5 µm were obtained and observed with ImageJ (National
684 Institute of Mental Health, Bethesda, Malyland, USA). The primary antibodies used were
685 rabbit anti-Myosin VIIa (Myo7a) (Proteus Biosciences, #25-6790), mouse anti-contactin-
686 associated protein (Caspr1) (Neuromab #75-001), guinea pig anti calretinin (Synaptic Systems
687 #214-104) and goat anti-osteopontin (Spp1) (R&D Systems #AF08). Their respective

688 secondary antibodies were Dylight 405 donkey anti-rabbit ifG H+L (Jackson Immuno Research
689 #711-475-152, Alexa Fluor 488 donkey anti-mouse IgG H+L (Life Technologies #A21202), Alexa
690 Fluor donkey anti-guinea-pig IgG H+L (Jackson ImmunoResearch #706-605-148) and Alexa
691 Fluor 555 donkey anti-goat IgG H+L (Invitrogen #A21432).
692 The hair cells in two vestibular organs (horizontal semi-circular canals and utricule) were
693 counted in the W6 group and the W12 group. The global number of hair cells was assessed
694 with the cytoplasmic labelling of the anti-Myo7a antibody (Hasson et al., 1997). Type I HC
695 were labelled using two different antibodies: anti-Spp1 in the neck of the type I HC (McInturff
696 et al., 2018) and the presence of anti-Caspr1 in the calyceal junctions of the calyx (Sousa et
697 al., 2009 p.20). Type II HC were distinguished by the colocalization of Myo7a and calretinin
698 (Maroto et al, 2021).
699
700 **Statistical analysis**
701 For both OKR and VOR stimulations, the effect of the protocol on the gain and phase were
702 statistically tested by performing repeated measures ANOVA. The *treatment* (SHAM or IDPN)
703 was considered as between individual independent factor with the *Weeks* (W0, W2, W4, W6,
704 W8, W10, W12) and the *Frequencies* (0.1, 0.2, 0.33, 0.5 and 1Hz for the OKR; 0.2, 0.5, 0.8, 1
705 and 2Hz for the VOR) were considered as within individual independent factors. The main
706 effects of those factors and their interactions were tested and reported. In the case of the
707 OCR and OVAR, mix-model ANOVA was used with only *Weeks* considered as within factors.
708 For the CGR, measured at W6 and W12, mix-model ANOVA was used with the *Frequencies*
709 and *Model* (Measured or Model CGR) used as within factors. For the comparison between the
710 OKR and VOR Δ gain, a repeated measures ANOVA was applied on the Δ gain (Wx-W0) with
711 the *stimulation modality* (OKR or VOR) as between individual independent factor and the
712 *Weeks* as within individual independent factor. For the correlation between OCR and VOR, as
713 well as the measured and theoretical CGR gain a linear regression model was fitted.
714 The effect of IDPN exposure on the hair cell count was reported with a Kruskal Wallis test.
715 For all analyses the significance threshold was set at $p<0.05$ and Newman Keuls post hoc test
716 was performed if the main effect or an interaction was found significant.

717 **FIGURE LEGENDS**

718 Figure 1: Effects of subchronic IDPN on canal- and otolithic- dependent VOR.

719 **A)** Illustration of the angular horizontal vestibulo-ocular reflex (aVOR) set-up. All tests are
720 performed in complete dark**. B)** Examples of raw aVOR traces in response to table rotations
721 (1Hz at 30°/s) recorded in the dark in an IDPN mouse before (W0), after 6 weeks of treatment
722 (W6) and 6 weeks of washout (W12). Right movement is represented up. **C)** Mean aVOR gain
723 of SHAM (n=22) and IDPN (n=21) mice during the protocol. **D)** Illustration of the ocular-
724 counter roll (OCR) set-up. **E)** Angles of eye elevation in response to roll static angles, recorded
725 in the dark in an IDPN mouse before (W0), after 6 weeks of IDPN (W6) and 6 weeks of washout
726 (W12). Gain of the OCR is the slope of linear regression lines (W0: r^2=0.9614; W6: r^2=0.6670;
727 W12: r^2=0.9549). Inset: example of a raw trace of OCR at W0. Left table roll (represented
728 negative) leads to left eye elevation (represented positive). **F)** Mean OCR gain of SHAM (n=14)
729 and IDPN (n=13) mice. We note that there was a significant difference between SHAM and
730 IDPN during the initial measurements at W0. However, at this time point mice were not yet
731 separated into different groups. This incidental difference completely disappeared on the
732 measurement performed at W2. (*p< 0.05; **p < 0.01; ***p < 0,001). Error bars represent
733 ±SEM.

734

735 Figure 2: Comparison of the dynamics of canalar and otolithic loss of function.

736 **A)** Evolution of the Mean Gain of the aVOR (1Hz) and OCR responses of IDPN mice (n=13)
737 during the treatment and washout periods. **B)** Individual gains for 1Hz aVOR (left) and OCR
738 (right) of the 13 IDPN mice, identified with similar symbols. The grey symbols in the left panel
739 correspond to aVOR gain values associated with VAF<0.5. **C, D**) Individual ΔaVOR gains as a
740 function of individual ΔOCR gains at W6 (C) and W12 (D) compared to W0, for SHAM (n=14)
741 and IDPN (n=13) mice. The linear regression corresponds to IDPN values is represented, as
742 well as the 50% confidence interval of each group (shaded areas). The symbols for each
743 animal are the same in panels B, C and D. (*p< 0.05; **p < 0.01; ***p < 0.001). Error bars
744 represent ±SEM.

745

746 Figure 3: Immuno-labelling of hair cells in the central regions of the horizontal SCC ampulla
747 and striolar region of the utricule Macula.

748 **A, B)** Immunolabelling of type I HC (Spp1+ and Caspr1+), type II HC (Calre +), or all HC (Myo7a)
749 for the SHAM, IDPN W6 and IDPN W12 groups in the central ampulla of the horizontal canal
750 (A1) and central utricular maculae (B1). Cell count at W6 and W12 in the central horizontal
751 ampulla (A2 and A3) and central utricular maculae (B2 and B3). **C1, C3)** Individual number of
752 central Spp1+ type I HC, Caspr1 + type I HC and Calre+ type II HC, or all HC(Myo7a) as a
753 function of the aVOR gain (C1) or OCR gain (C2) at W6 (circle) and W12 (squares) groups. The
754 linear regressions correspond to all individuals (n=23 mice). **C2, C4)** Comparison of the
755 number of Caspr1 type I HC as a function of the aVOR (C2) gain or OCR gain (C4) at W6 (black
756 and circle) and at W12 (pink and square) for each IDPN mice of the W12 group (n=8). Note
757 that all points are shifted toward the regression line (redrawn from respectively C1 and C3),
758 indicating that the number of cells at W12 better correlates with the recovered aVOR. (*p<
759 0.05; **p < 0.01; ***p < 0,001). Error bars represent ±SEM.
760
761 <u>Figure 4: Effects of subchronic IDPN treatment on the OKR.</u>
762 **A)** Illustration of the optokinetic reflex (OKR) set-up. **B)** Example of raw traces of an OKR
763 recorded in response to stimulation at 0.5Hz &10°/s before (W0), after 4 weeks of IDPN
764 treatment (W4), 2 weeks (W8) and 6 weeks of washout (W12). All traces are from the same
765 individual. **C)** Mean OKR gain of IDPN (n=12) and SHAM (n=12) mice. **D)** OKR gain and (E) phase
766 for IDPN (n=12) and SHAM (n=12) for each frequency at W0, W6, W8 and W12. (*p< 0.05; **p
767 < 0.01; ***p < 0,001). Error bars represent ±SEM.
768
769 <u>Figure 5: Comparison of the IDPN treatment on OKR and aVOR.</u>
770 **A)** Mean Δ aVOR and Δ Gain for 0.2, 0.5 and 1Hz for IDPN (n=12) and SHAM (n=12) mice. **B)**
771 Individual ΔaVOR gains as a function of individual ΔOKR gains. The 50% confidence interval of
772 each group is represented in the shaded areas. **C)** aVOR and OKR gains of IDPN mice (n=12)
773 at W0 and W8 for frequencies of 0.2, 0.5 and 1Hz. **D)** Percentage of the individual vestibular
774 weight (inset), as a function of the percentage of the individual OKR gains change for IDPN
775 (n=12). The linear regression corresponds to all values (n=36). (*p< 0.05; **p < 0.01; ***p <
776 0,001). Error bars represent ±SEM.
777
778 <u>Figure 6: Visuo-Vestibular interactions following IDPN treatment.</u>

A) aVOR, OKR, CGR data (CGR) and predicted CGR (MODEL) gains (left panel), and CGR phase (data and model, right panel), for the SHAM mice (n=12). **B)** aVOR, OKR, CGR data (CGR) and predicted CGR (MODEL) gains for the IDPN mice (n=19). **C)** Comparison of the predicted versus measured CGR for all frequencies tested. The dotted line at 45° represents a perfect match between prediction and data (optimal CGR). **D)** aVOR, OKR, and CGR values of the IDPN mice (n=19) (left panel). Clustering analysis (right panel) distinguish 2 groups based on Δ, and a subgroup based on VOR. The horizontal coordinate of each cluster (vertical lines) represents the distance between two connected clusters. **E)** Delta (CGR-OKR) as a function of the VOR Sweep Amplitude of the Δ+ (green triangle), Δ+(-) (green diamonds) and Δ- (orange) IDPN mice. The inset panel represents typical raw cycles representative of the 3 subgroups. **F)** Delta (CGR-OKR) as a function of the VOR reproducibility of the Δ+ (green triangle), Δ+(-) (green diamonds) and Δ- (orange) IDPN mice. Regression line correspond to all values (n=19)

TABLES

Table 1 Statistics table of the aVOR gain for the IDPN treated group.

W0	W2	W4	W6	W8	W10	W12	
	ns	***	***	***	***	***	W0
ns		***	***	***	***	***	W2
***	***		***	***	ns	ns	W4
***	***	***		*	***	***	W6
***	***	***	*		***	***	W8
***	***	ns	***	***		ns	W10
***	***	ns	***	***	ns		W12

Table 2: Statistics table of the OKR gain for the IDPN treated group.

W0	W2	W4	W6	W8	W10	W12	
	ns	ns	ns	***	ns	ns	W0
ns		ns	ns	***	**	ns	W2
ns	ns		ns	ns	ns	ns	W4
ns	ns	ns		*	ns	ns	W6
***	***	ns	*		ns	ns	W8
ns	**	ns	ns	ns		ns	W10
ns	ns	ns	ns	ns	ns		W12

References

Agrawal Y, Carey JP, Della Santina CC, Schubert MC, Minor LB (2009) Disorders of Balance and Vestibular Function in US Adults: Data From the National Health and Nutrition Examination Survey, 2001-2004. Arch Intern Med 169:938.

Agrawal Y, Ward BK, Minor LB (2013) Vestibular dysfunction: Prevalence, impact and need for targeted treatment Chabbert C, ed. J Vestib Res 23:113–117.

Beraneck M, Bojados M, Le Séac'h A, Jamon M, Vidal P-P (2012) Ontogeny of Mouse Vestibulo-Ocular Reflex Following Genetic or Environmental Alteration of Gravity Sensing Gilestro GF, ed. PLoS ONE 7:e40414.

Beraneck M, Cullen KE (2007) Activity of Vestibular Nuclei Neurons During Vestibular and Optokinetic Stimulation in the Alert Mouse. J Neurophysiol 98:1549–1565.

Beraneck M, Idoux E (2012) Reconsidering the Role of Neuronal Intrinsic Properties and Neuromodulation in Vestibular Homeostasis. Front Neurol 3 Available at: http://journal.frontiersin.org/article/10.3389/fneur.2012.00025/abstract.

Beraneck M, Pfanzelt S, Vassias I, Rohregger M, Vibert N, Vidal P-P, Moore LE, Straka H (2007) Differential Intrinsic Response Dynamics Determine Synaptic Signal Processing in Frog Vestibular Neurons. J Neurosci 27:4283–4296.

Beraneck M, Straka H (2011) Vestibular signal processing by separate sets of neuronal filters Peusner KD, ed. J Vestib Res 21:5–19.

Bisdorff A, Von Brevern M, Lempert T, Newman-Toker DE (2009) Classification of vestibular symptoms: Towards an international classification of vestibular disorders. J Vestib Res 19:1–13.

Boadas-Vaello P, Sedó-Cabezón L, Verdú E, Llorens J (2017) Strain and Sex Differences in the Vestibular and Systemic Toxicity of 3,3′-Iminodipropionitrile in Mice. Toxicol Sci:kfw238.

Boyden ES, Katoh A, Raymond JL (2004) CEREBELLUM-DEPENDENT LEARNING: The Role of Multiple Plasticity Mechanisms. Annu Rev Neurosci 27:581–609.

Boyle R, Carey JP, Highstein SM (1991) Morphological correlates of response dynamics and efferent stimulation in horizontal semicircular canal afferents of the toadfish, Opsanus tau. J Neurophysiol 66:1504–1521.

Brandt T, Dieterich M (2017) The dizzy patient: don't forget disorders of the central vestibular system. Nat Rev Neurol 13:352–362.

Brandt T, Strupp M, Arbusow V, Dieringer N (1997) Plasticity of the vestibular system: central compensation and sensory substitution for vestibular deficits. Adv Neurol:297–309.

Brueckner JK, Ashby LP, Prichard JR, Porter JD (1999) Vestibulo-ocular pathways modulate extraocular muscle myosin expression patterns. Cell Tissue Res 295:477–484.

Carcaud J, França de Barros F, Idoux E, Eugène D, Reveret L, Moore LE, Vidal P-P, Beraneck M (2017) Long-Lasting Visuo-Vestibular Mismatch in Freely-Behaving Mice Reduces the Vestibulo-Ocular Reflex and Leads to Neural Changes in the Direct Vestibular Pathway. eneuro 4:ENEURO.0290-16.2017.

Carey JP, Fuchs AF, Rubel EW (1996) Hair cell regeneration and recovery of the vestibuloocular reflex in the avian vestibular system. J Neurophysiol 76:3301–3312.

Carriot J, Jamali M, Chacron MJ, Cullen KE (2017) The statistics of the vestibular input experienced during natural self-motion differ between rodents and primates: Natural vestibular input in rodents and monkeys. J Physiol 595:2751–2766.

Cassel R, Bordiga P, Carcaud J, Simon F, Beraneck M, Le Gall A, Benoit A, Bouet V, Philoxene B, Besnard S, Watabe I, Pericat D, Hautefort C, Assie A, Tonetto A, Dyhrfjeld-Johnsen J, Llorens J, Tighilet B, Chabbert C (2019) Morphological and functional correlates of vestibular synaptic deafferentation and repair in a mouse model of acute onset vertigo. Dis Model Mech:dmm.039115.

Contini D, Holstein GR, Art JJ (2022) Simultaneous Dual Recordings From Vestibular Hair Cells and Their Calyx Afferents Demonstrate Multiple Modes of Transmission at These Specialized Endings. Front Neurol 13:891536.

Cullen K (2019) Vestibular processing during natural self-motion: implications for perception and action. :41.

Cullen KE, Minor LB, Beraneck M, Sadeghi SG (2010) Neural substrates underlying vestibular compensation: Contribution of peripheral versus central processing. J Vestib Res 19:171–182.

De Zeeuw CI, Lisberger SG, Raymond JL (2021) Diversity and dynamism in the cerebellum. Nat Neurosci 24:160–167.

Dean P, Porrill J (2014) Decorrelation Learning in the Cerebellum. In: Progress in Brain Research, pp 157–192. Elsevier. Available at: https://linkinghub.elsevier.com/retrieve/pii/B9780444633569000078.

Eatock RA, Songer JE (2011) Vestibular Hair Cells and Afferents: Two Channels for Head Motion Signals. Annu Rev Neurosci 34:501–534.

Ernst MO, Banks MS (2002) Humans integrate visual and haptic information in a statistically optimal fashion. Nature 415:429–433.

Facchini J, Rastoldo G, Xerri C, Péricat D, El Ahmadi A, Tighilet B, Zennou-Azogui Y (2021) Unilateral vestibular neurectomy induces a remodeling of somatosensory cortical maps. Prog Neurobiol 205:102119.

Faulstich BM, Onori KA, du Lac S (2004) Comparison of plasticity and development of mouse optokinetic and vestibulo-ocular reflexes suggests differential gain control mechanisms. Vision Res 44:3419–3427.

Faulstich M, van Alphen AM, Luo C, du Lac S, De Zeeuw CI (2006) Oculomotor Plasticity During Vestibular Compensation Does Not Depend on Cerebellar LTD. J Neurophysiol 96:1187–1195.

Fetsch CR, DeAngelis GC, Angelaki DE (2010) Visual-vestibular cue integration for heading perception: applications of optimal cue integration theory: Mechanisms of visual-vestibular cue integration. Eur J Neurosci 31:1721–1729.

França de Barros F, Carcaud J, Beraneck M (2019) Long-term Sensory Conflict in Freely Behaving Mice. J Vis Exp:59135.

França de Barros F, Schenberg L, Tagliabue M, Beraneck M (2020) Long term visuo-vestibular mismatch in freely behaving mice differentially affects gaze stabilizing reflexes. Sci Rep 10:20018.

Glasauer S (2007) Current Models of the Ocular Motor System. In: Developments in Ophthalmology, 2007 (Straube A, Büttner U, eds), pp 158–174. Basel: KARGER. Available at: https://www.karger.com/Article/FullText/100485.

Goldberg JM (2000) Afferent diversity and the organization of central vestibular pathways. Exp Brain Res 130:277–297.

González-Calvo I et al. (2021) Sushi domain-containing protein 4 controls synaptic plasticity and motor learning. eLife 10:e65712.

Greguske EA, Carreres-Pons M, Cutillas B, Boadas-Vaello P, Llorens J (2019) Calyx junction dismantlement and synaptic uncoupling precede hair cell extrusion in the vestibular sensory epithelium during sub-chronic 3,3′-iminodipropionitrile ototoxicity in the mouse. Arch Toxicol 93:417–434.

Greguske EA, Llorens J, Pyott SJ (2021) Assessment of cochlear toxicity in response to chronic 3,3′-iminodipropionitrile in mice reveals early and reversible functional loss that precedes overt histopathology. Arch Toxicol 95:1003–1021.

Grosch M, Lindner M, Bartenstein P, Brandt T, Dieterich M, Ziegler S, Zwergal A (2021) Dynamic whole-brain metabolic connectivity during vestibular compensation in the rat. NeuroImage 226:117588.

Hasson T, Gillespie PG, Garcia JA, MacDonald RB, Zhao Y, Yee AG, Mooseker MS, Corey DP (1997) Unconventional Myosins in Inner-Ear Sensory Epithelia. J Cell Biol 137:1287–1307.

Hess BJM, Dieringer N (1990) Spatial Organization of the Maculo-Ocular Reflex of the Rat: Responses During Off-Vertical Axis Rotation. Eur J Neurosci 2:909–919.

Highstein SM, Goldberg JM, Moschovakis AK, Fernandez C (1987) Inputs from regularly and irregularly discharging vestibular nerve afferents to secondary neurons in the vestibular nuclei of the squirrel monkey. II. Correlation with output pathways of secondary neurons. J Neurophysiol 58:719–738.

Holland PJ, Sibindi TM, Ginzburg M, Das S, Arkesteijn K, Frens MA, Donchin O (2020) A Neuroanatomically Grounded Optimal Control Model of the Compensatory Eye Movement System in Mice. Front Syst Neurosci 14:13.

Idoux E, Tagliabue M, Beraneck M (2018) No Gain No Pain: Relations Between Vestibulo-Ocular Reflexes and Motion Sickness in Mice. Front Neurol 9:918.

Jang DC, Shim HG, Kim SJ (2020) Intrinsic Plasticity of Cerebellar Purkinje Cells Contributes to Motor Memory Consolidation. J Neurosci 40:4145–4157.

Kim GS, Wang T, Sayyid ZN, Fuhriman J, Jones SM, Cheng AG (2022) Repair of surviving hair cells in the damaged mouse utricle. Proc Natl Acad Sci 119:e2116973119.

Kodama T, du Lac S (2016) Adaptive Acceleration of Visually Evoked Smooth Eye Movements in Mice. J Neurosci 36:6836–6849.

Lasker DM, Han GC, Park HJ, Minor LB (2008) Rotational Responses of Vestibular–Nerve Afferents Innervating the Semicircular Canals in the C57BL/6 Mouse. J Assoc Res Otolaryngol 9:334–348.

Leong ATL, Gu Y, Chan Y-S, Zheng H, Dong CM, Chan RW, Wang X, Liu Y, Tan LH, Wu EX (2019) Optogenetic fMRI interrogation of brain-wide central vestibular pathways. Proc Natl Acad Sci 116:10122–10129.

Llorens J, Demêmes D (1994) Hair cell degeneration resenting from 3,3'-imiodiprpiunitril toxicity in the rat vestibular epithelia. Hear Res:78–86.

Llorens J, Demêmes D, Sans A (1993) The behavioural syndrome caused by 3'3-Iminodipropionitrile and related nitriles in the rat is associated with degeneration of the vestibular sensory hair cells. Toxicol Appl Pharmacol:199–210.

Llorens J, Demêmes D, Sans A (1994) The toxicity of IDPN on the vestibular system of the rat: new insights on its effects on behavior and neurofilament transport. NeuroToxicology:643–647.

Lopez C, Schreyer H-M, Preuss N, Mast FW (2012) Vestibular stimulation modifies the body schema. Neuropsychologia 50:1830–1837.

Lopez-Escamez JA, Carey J, Chung W-H, Goebel JA, Magnusson M, Mandalà M, Newman-Toker DE, Strupp M, Suzuki M, Trabalzini F, Bisdorff A (2015) Diagnostic criteria for Menière's disease. J Vestib Res 25:1–7.

Maroto AF, Barrallo-Gimeno A, Llorens J (2021) Relationship between vestibular hair cell loss and deficits in two anti-gravity reflexes in the rat. Hear Res 410:108336.

Martins-Lopes V, Bellmunt A, Greguske EA, Maroto AF, Boadas-Vaello P, Llorens J (2019a) Quantitative Assessment of Anti-Gravity Reflexes to EvaluateVestibular Dysfunction in Rats. J Assoc Res Otolaryngol 20:553–563.

Martins-Lopes V, Bellmunt A, Greguske EA, Maroto AF, Boadas-Vaello P, Llorens J (2019b) Quantitative Assessment of Anti-Gravity Reflexes to EvaluateVestibular Dysfunction in Rats. J Assoc Res Otolaryngol 20:553–563.

McInturff S, Burns JC, Kelley MW (2018) Characterization of spatial and temporal development of Type I and Type II hair cells in the mouse utricle using new cell-type-specific markers. Biol Open 7:bio038083.

Minor L, Goldberg J (1991) Vestibular-nerve inputs to the vestibulo-ocular reflex: a functional- ablation study in the squirrel monkey. J Neurosci 11:1636–1648.

Möhwald K, Hadzhikolev H, Bardins S, Becker-Bense S, Brandt T, Grill E, Jahn K, Dieterich M, Zwergal A (2020) Health-related quality of life and functional impairment in acute vestibular disorders. Eur J Neurol 27:2089–2098.

Nelson AB, Faulstich M, Moghadam S, Onori K, Meredith A, du Lac S (2017) BK Channels Are Required for Multisensory Plasticity in the Oculomotor System. Neuron 93:211–220.

Oommen BS, Stahl JS (2008) Eye orientation during static tilts and its relationship to spontaneous head pitch in the laboratory mouse. Brain Res 1193:57–66.

Pfanzelt S, Rossert C, Rohregger M, Glasauer S, Moore LE, Straka H (2008) Differential Dynamic Processing of Afferent Signals in Frog Tonic and Phasic Second-Order Vestibular Neurons. J Neurosci 28:10349–10362.

Sadeghi SG, Beraneck M (2020) Task-Specific Differentiation of Central Vestibular Neurons and Plasticity During Vestibular Compensation. In: The Senses: A Comprehensive Reference, pp 290–308. Elsevier. Available at: https://linkinghub.elsevier.com/retrieve/pii/B978012809324524145X

Sadeghi SG, Minor LB, Cullen KE (2007) Response of Vestibular-Nerve Afferents to Active and Passive Rotations Under Normal Conditions and After Unilateral Labyrinthectomy. J Neurophysiol 97:1503–1514.

Sadeghi SG, Minor LB, Cullen KE (2012) Neural Correlates of Sensory Substitution in Vestibular Pathways following Complete Vestibular Loss. J Neurosci 32:14685–14695.

Sayyid ZN, Wang T, Chen L, Jones SM, Cheng AG (2019) Atoh1 Directs Regeneration and Functional Recovery of the Mature Mouse Vestibular System. Cell Rep 28:312-324.e4.

Sedó-Cabezón L, Boadas-Vaello P, Soler-Martín C, Llorens J (2014) Vestibular damage in chronic ototoxicity: A mini-review. NeuroToxicology 67.

Sedó-Cabezón L, Jedynak P, Boadas-Vaello P, Llorens J (2015) Transient alteration of the vestibular calyceal junction and synapse in response to chronic ototoxic insult in rats. Dis Model Mech:dmm.021436.

Seoane A, Demêmes D, Llorens J (2001) Pathology of the rat vestibular sensory epithelia during subchronic 3,3′-iminodipropionitrile exposure: hair cells may not be the primary target of toxicity. Acta Neuropathol (Berl) 102:339–348.

Shin S-L, Zhao GQ, Raymond JL (2014) Signals and Learning Rules Guiding Oculomotor Plasticity. J Neurosci 34:10635–10644.

Shinder ME, Perachio AA, Kaufman GD (2005) VOR and Fos response during acute vestibular compensation in the Mongolian gerbil in darkness and in light. Brain Res 1038:183–197.

Simon F, Pericat D, Djian C, Fricker D, Denoyelle F, Beraneck M (2020) Surgical techniques and functional evaluation for vestibular lesions in the mouse: unilateral labyrinthectomy (UL) and unilateral vestibular neurectomy (UVN). J Neurol 267:51–61.

Simon F, Tissir F, Michel V, Lahlou G, Deans M, Beraneck M (2021) Implication of Vestibular Hair Cell Loss of Planar Polarity for the Canal and Otolith-Dependent Vestibulo-Ocular Reflexes in Celsr1–/– Mice. Front Neurosci 15:750596.

Soler-Martin C, Diez-Padrisa N, Boadas-Vaello P, Llorens J (2006) Behavioral Disturbances and Hair Cell Loss in the Inner Ear Following Nitrile Exposure in Mice, Guinea Pigs, and Frogs. Toxicol Sci 96:123–132.

Sousa AD, Andrade LR, Salles FT, Pillai AM, Buttermore ED, Bhat MA, Kachar B (2009) The Septate Junction Protein Caspr Is Required for Structural Support and Retention of KCNQ4 at Calyceal Synapses of Vestibular Hair Cells. J Neurosci 29:3103–3108.

Straka H, Vibert N, Vidal PP, Moore LE, Dutia MB (2005) Intrinsic membrane properties of vertebrate vestibular neurons: Function, development and plasticity. Prog Neurobiol 76:349–392.

Straka H, Zwergal A, Cullen KE (2016) Vestibular animal models: contributions to understanding physiology and disease. J Neurol 263:10–23.

Wibble T, Pansell T, Grillner S, Pérez-Fernández J (2022) Conserved subcortical processing in visuo-vestibular gaze control. Nat Commun 13:4699.

Wilkerson BA, Artoni F, Lea C, Ritchie K, Ray CA, Bermingham-McDonogh O (2018) Effects of 3,3′-Iminodipropionitrile on Hair Cell Numbers in Cristae of CBA/CaJ and C57BL/6J Mice. J Assoc Res Otolaryngol 19:483–491.

Yang X, Zhou S, Wu J, Liao Q, Wang C, Liu M, Qu L, Zhang Y, Cheng C, Chai R, Zhang K, Yu X, Huang P, Liu L, Xiong W, Chen S, Chen F (2019) Surgery-free video-oculography in mouse models: enabling quantitative and short-interval longitudinal assessment of vestibular function. Neurosci Lett 696:212–218.

Zakir M, Dickman JD (2006) Regeneration of Vestibular Otolith Afferents after Ototoxic Damage. J Neurosci 26:2881–2893.

Zeng S, Ni W, Jiang H, You D, Wang J, Lu X, Liu L, Yu H, Wu J, Chen F, Li H, Wang Y, Chen Y, Li W (2020) Toxic Effects of 3,3 ′ -Iminodipropionitrile on Vestibular System in Adult C57BL/6J Mice *In Vivo*. Neural Plast 2020:1–11.

Zennou-Azogui Y, Xerri C, Harlay F (1994) Visual sensory substitution in vestibular compensation: neuronal substrates in the alert cat. Exp Brain Res 98 Available at: http://link.springer.com/10.1007/BF00233983.

Zwergal A, Schlichtiger J, Xiong G, Beck R, Günther L, Schniepp R, Schöberl F, Jahn K, Brandt T, Strupp M, Bartenstein P, Dieterich M, Dutia MB, la Fougère C (2016) Sequential [18F]FDG µPET whole-brain imaging of central vestibular compensation: a model of deafferentation-induced brain plasticity. Brain Struct Funct 221:159–170.

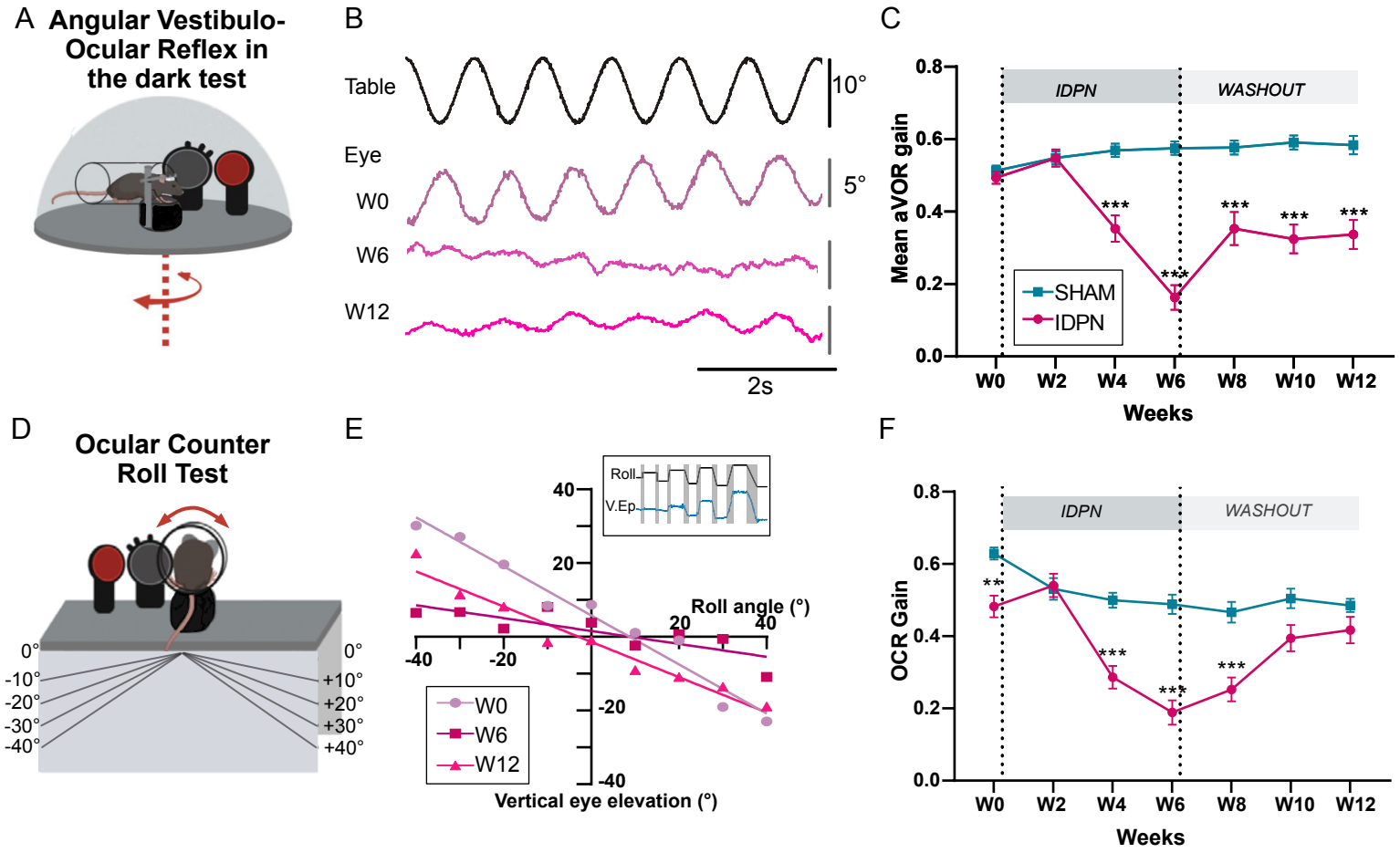

Figure 1: Effects of subchronic IDPN on canal- and otolithic- dependent VOR.

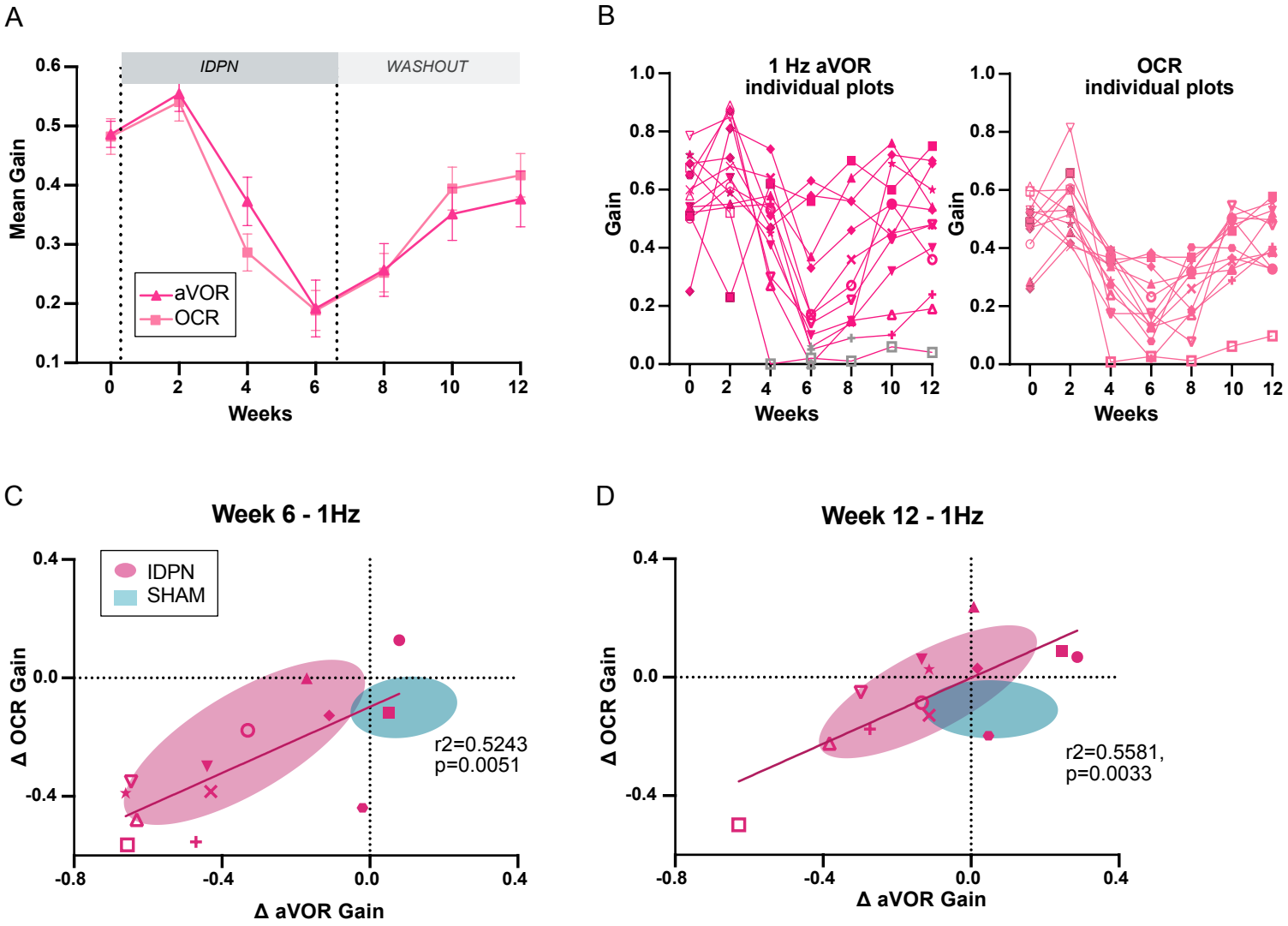

Figure 2: Comparison of the dynamics of canalar and otolithic loss of function.

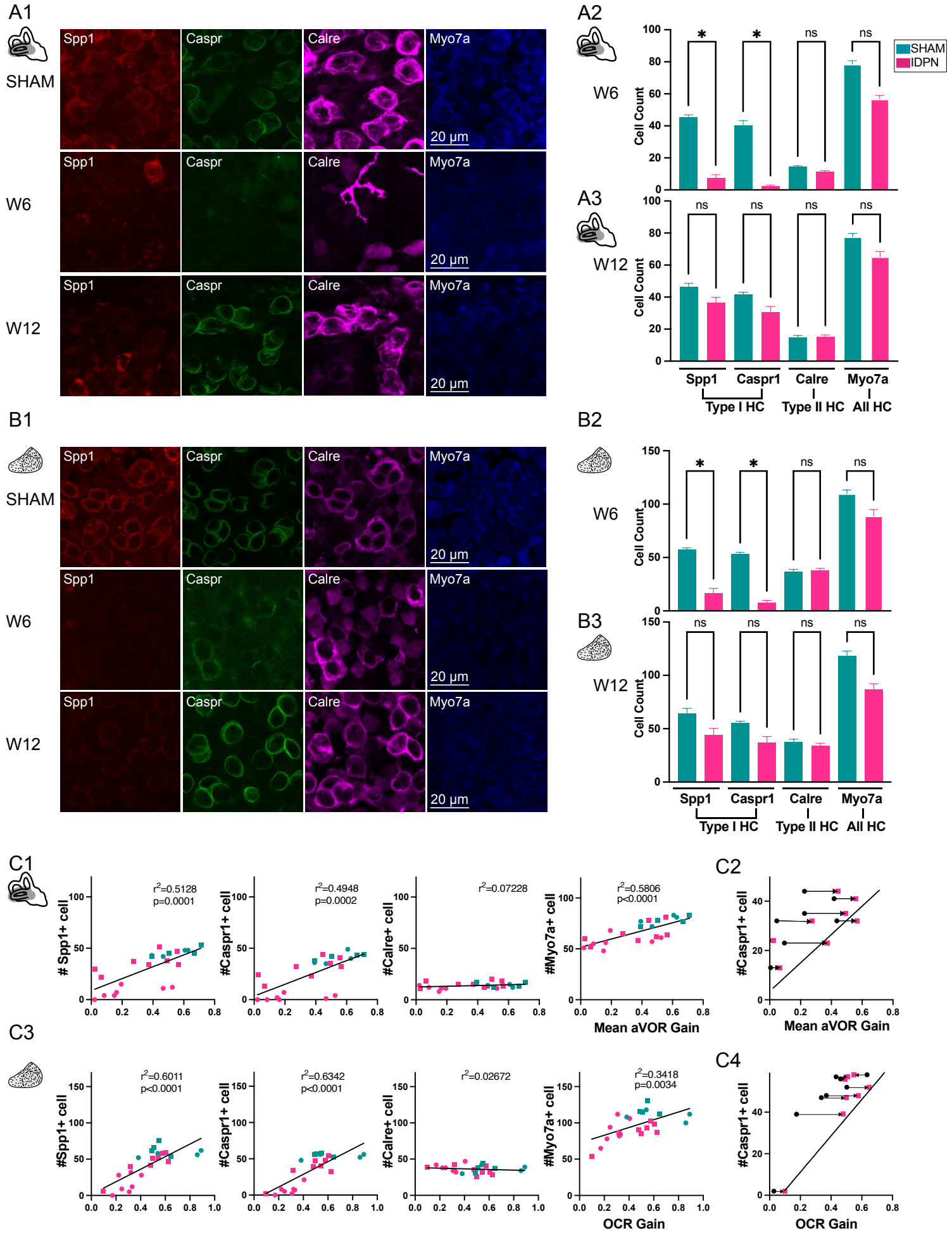

Figure 3: Immuno-labelling of hair cells in the central regions of the horizontal SCC ampulla and striolar region of the utricule Macula.

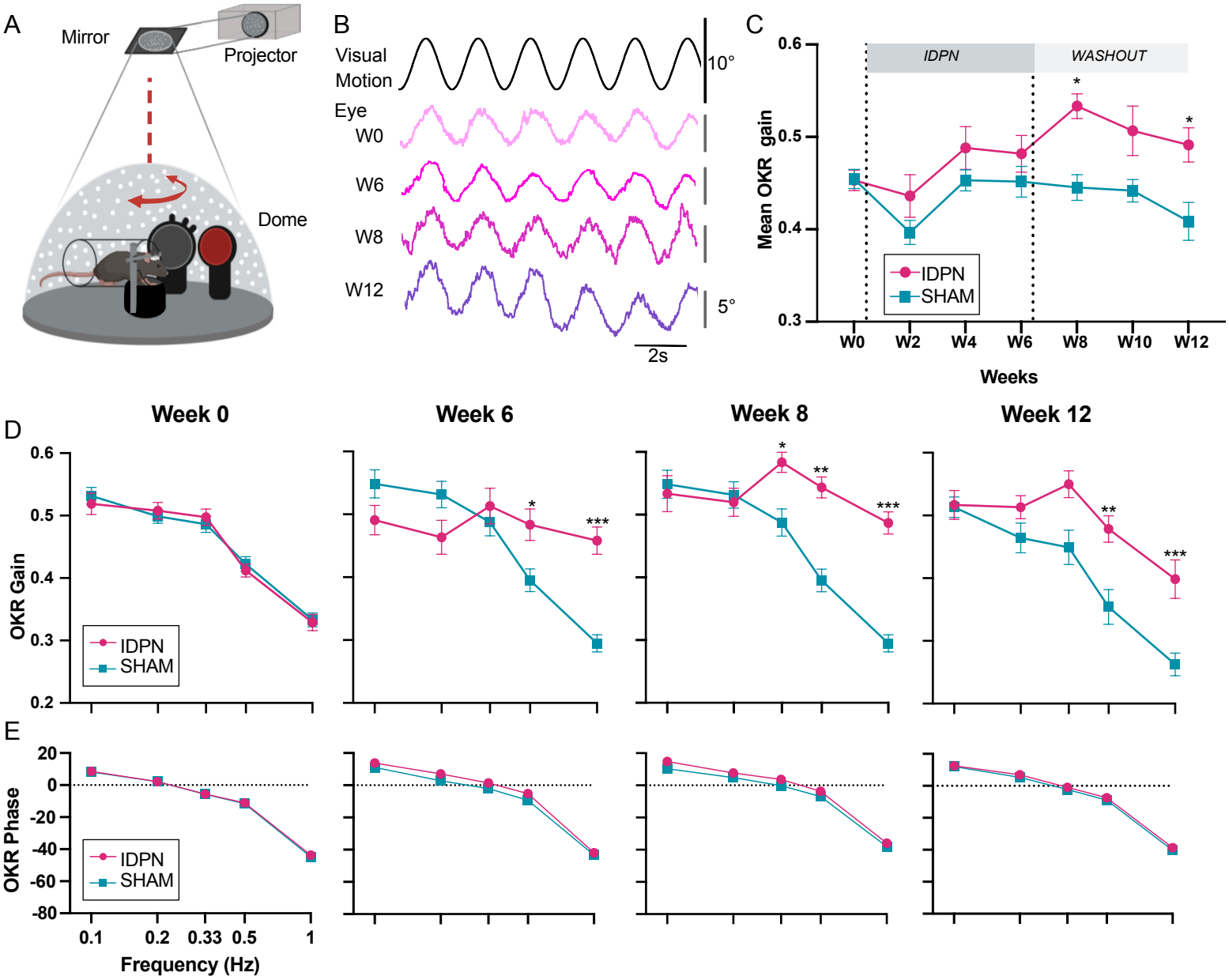

Figure 4: Effects of subchronic IDPN treatment on the OKR.

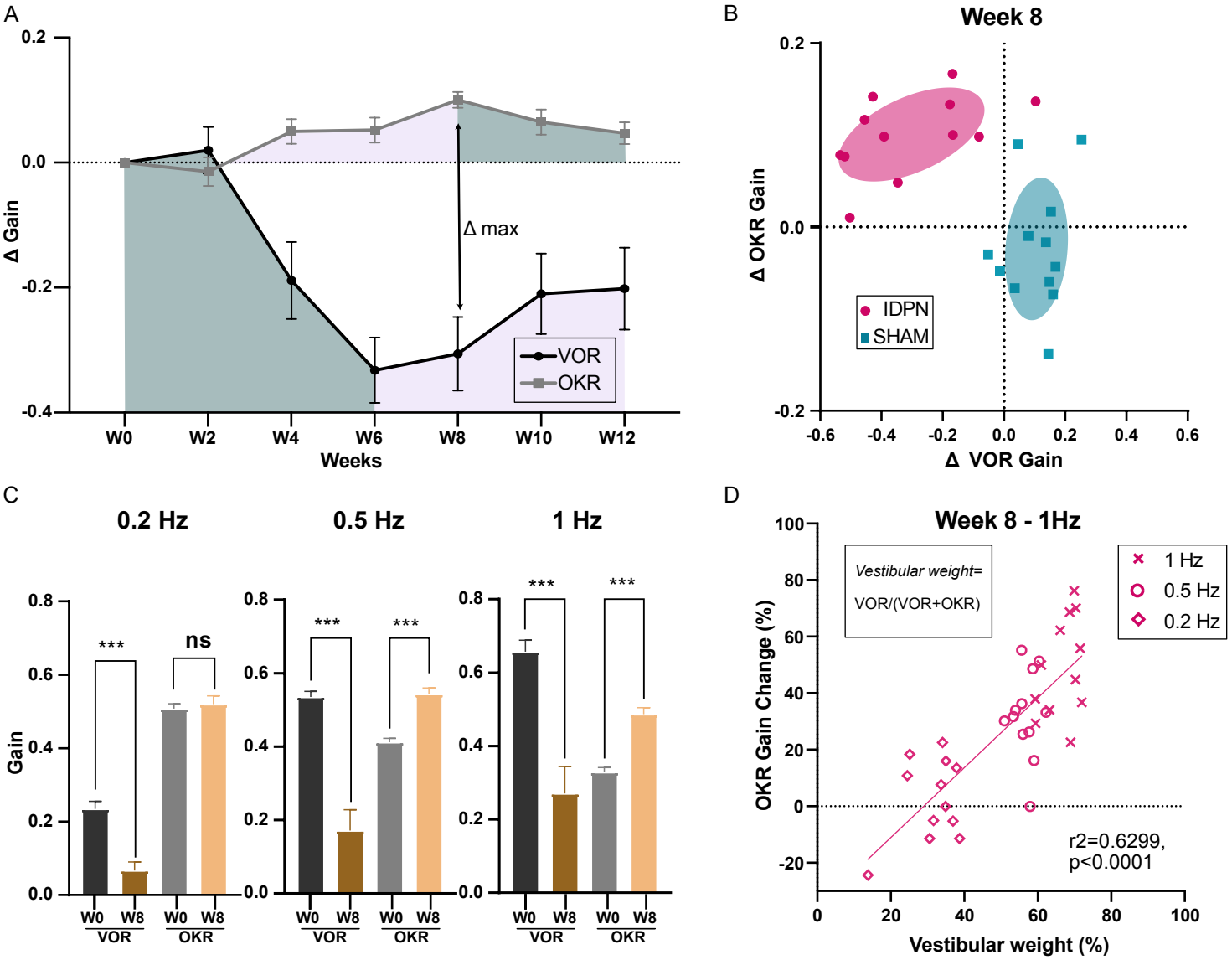

Figure 5: Comparison of the IDPN treatment on OKR and aVOR.

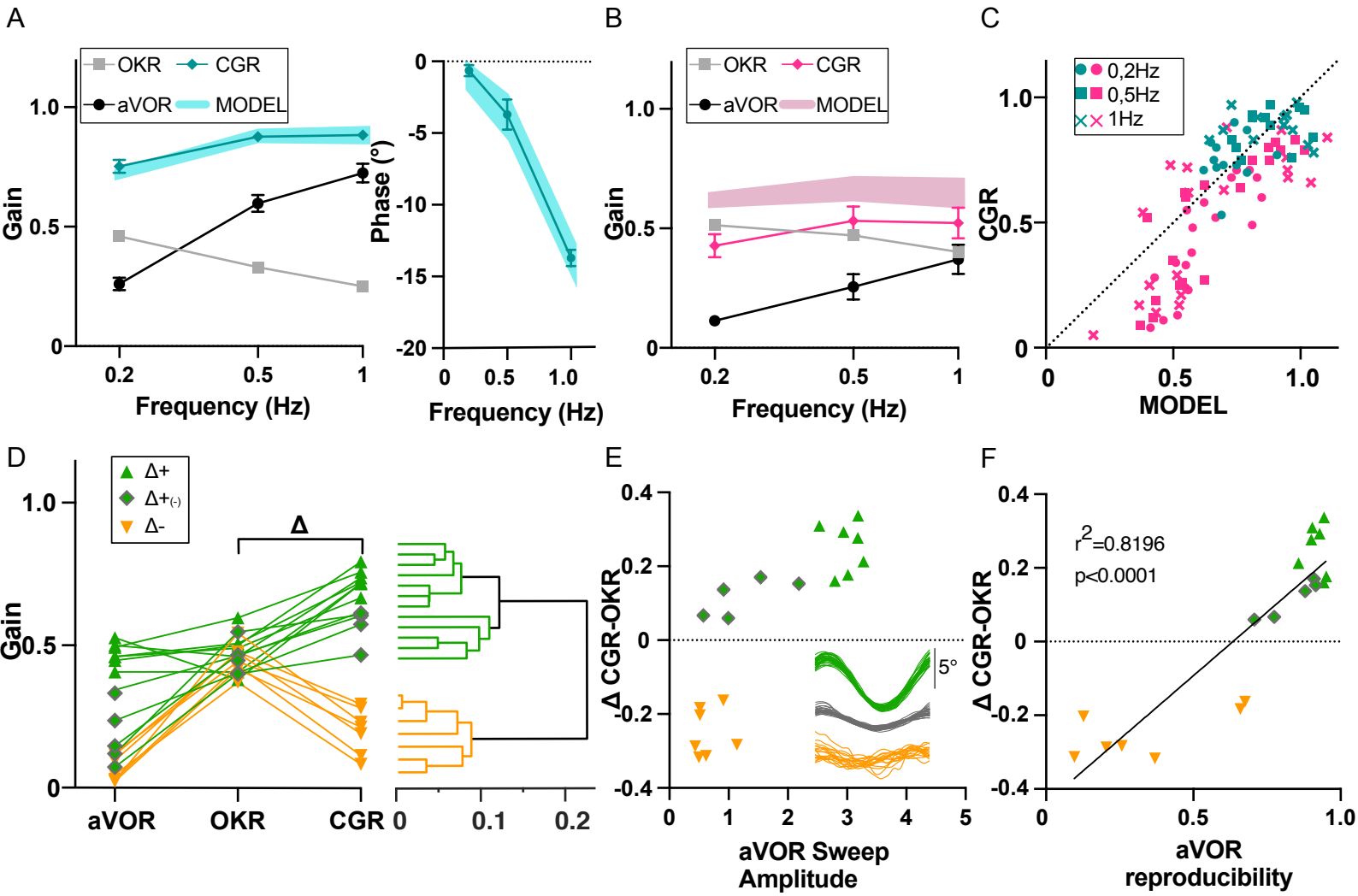

Figure 6: Visuo-vestibular interactions following IDPN treatment.